FLOW CONTROL VIA SYNTHETIC JET ACTUATION

A Thesis

by

ADAM COLE MILLER

Submitted to the Office of Graduate Studies of
Texas A&M University
in partial fulfillment of the requirements for the degree of

MASTER OF SCIENCE

December 2004

Major Subject: Aerospace Engineering

FLOW CONTROL VIA SYNTHETIC JET ACTUATION

A Thesis

by

ADAM COLE MILLER

Submitted to Texas A&M University
in partial fulfillment of the requirements
for the degree of

MASTER OF SCIENCE

Approved as to style and content by:

Othon K. Rediniotis
(Chair of Committee)

Paul G. Cizmas
(Member)

Luis San Andres
(Member)

Walter Haisler
(Head of Department)

December 2004

Major Subject: Aerospace Engineering

ABSTRACT

Flow Control via Synthetic Jet Actuation. (December 2004)
Adam Cole Millar, B.S., Texas A&M University
Chair of Advisory Committee: Dr. Othon K. Rediniotis

An experimental investigation was undertaken to determine the ability of Synthetic Jet Actuators to control the aerodynamic properties of a wing. The Synthetic Jet Actuator (SJA) was placed at two separate positions on a wing comprised of a NACA0015 airfoil. The first of the jet positions is located at 12% of the chord, hereby referred to as the leading edge Synthetic Jet Actuator. The second exit position is located at 99% chord of an airfoil and hereby is referred to as the trailing edge Synthetic Jet Actuator. The two locations produced different benefits as the angle of attack of the wing was increased.

The leading edge Synthetic Jet Actuator delayed the onset of stall of an airfoil, suppressing stall up to 25 degrees angle of attack. The control of the aerodynamic characteristics was achieved by influencing the amount of the separated flowfield region. The effects of the dynamic stall vortex were investigated with wind tunnel testing during the pitching motion of an airfoil to determine how the flow reacts dynamically.

The trailing edge synthetic jet actuator was investigated as a form of low angle "hinge-less" control. The study investigated the effect of the jet momentum coefficient on the ability of the synthetic jet to modify the lifting and pitching moment produced from the wind tunnel model. The data indicates that, with the present implementation, the SJA-jet flap generates moderate lift and moment coefficient increments that should be suitable for hinge-less control. It was also shown that, for the current experimental setup and a given jet momentum coefficient, continuous blowing is more effective than oscillatory

blowing/sucking. The data shows that combining the SJA with a Gurney flap does not result in performance enhancement.

DEDICATION

I dedicate this thesis to my mother and father, Charlotte and Billy Miller, for all of the patience and understanding to see reach this level of my education.

ACKNOWLEDGMENTS

I give a very large thanks to Dr. Othon Rediniotis, who has tolerated me for many years and has guided me on this educational journey. I would also like to thank Dr. Paul Cizmas who helped me enter graduate school and has been a friend ever since.

I thank the technical staff at Texas A&M for their patience and hard work. This includes Rick Allen, John Januskey, Josh Weimar and Rodney Inmon.

I greatly thank Dr. Lance W. Traub whose help has been invaluable these many years. His support has been helpful throughout the research process.

Lastly, I thank the Air Force, Dr. James Myatt and Dr. Chris Camphouse, for the generous SBIR grant that allows for funding of projects and research nationwide.

TABLE OF CONTENTS

Page

Page

LIST OF FIGURES

FIGURE Page

FIGURE Page

LIST OF TABLES

1. INTRODUCTION

General

This thesis presents a study of the effects of flow control on a NACA0015 airfoil using Synthetic Jet Actuators (SJA) at different locations along the chord. The purpose of this research was to show that fluid flow manipulation was achievable using these methods. The data taken from wind tunnel experimentation shows that these methods delayed the onset of stall and generated sufficient lift and moment to effectively control a wing. This study was broken into two major aspects of flow control: separation control and aerodynamic coefficient manipulation.

The benefits of flow control have become more important as the nature of aircraft changes. With the advent of stealth the need for a method of control with fixed surfaces has grown. Also, economic interests have demanded more weight savings in the interest of fuel economy. This demand has lead to the demand for increased lift-to-drag ratios. Synthetic jets have made it possible to protect an aircraft from flow separation thus staving off the undesirable effects of stall. Stall leads to loss in lift and a tremendous increase in drag forces.

This study focuses on the use of synthetic jet actuators to control the aerodynamic characteristics of a wing. This focus includes the pitching moment, the lift generated, and delaying separation causing an extension of the pre-stall angle of attack range. The goals are to eliminate, reduce, and manipulate the steady and unsteady flow separation over a wing, with active flow control and no control surfaces ("hinge-less" flow control). The manipulation of flow separation, and not the delay of separation, creates the possibilities of new alternatives over existing conventional surfaces. These advantages

This thesis follows the style and format of the Journal of Turbomachinery.

are that leading edge and trailing edge surfaces could be eliminated and that the aerodynamic loading over the wing area could be altered, providing a greater degree of control authority. With the advent of stealth technology, the need for aircraft to maintain a low level of radar observability has been greatly enhanced. This need creates an environment where the geometry of the vehicle has taken precedence over the aerodynamic performance. Aerodynamic flow control allows for an optimization of the aircraft without compromising the shape of the aircraft. This would allow the craft's radar signature to remain intact.

Control of Flow Separation

The stall of a wing or an aircraft is due to the separation of the flowfield over the surface the wing. Separation occurs because the flow in the boundary lacks the momentum to overcome the adverse pressure gradient. There are two main methods that have been used to delay stall in aircraft. These two types are known as active and passive techniques. Passive devices do not require any energy to be introduced. Passive devices that have been used for flow control include vortex generators [1], distributed roughness, acoustic cavities [2], and self excited rods [3]. Vortex generators enhance the mixing of the fluid in the shear layer. This mixing increases the amount of turbulence in the boundary layer and adds the energy needed to overcome the adverse pressure gradient. The other passive methods mentioned above function by natural tendencies inherent in the fluidic motion. These methods function by creating vortical structures in the flowfield by taking advantage of the harmonic receptivity of the flowfield. The vortical structures influence the mixing of fluid from the free stream velocity into the slower and lower energy boundary layer.

Active methods of stall control include suction [4,5], blowing [6], wall heating, moving surface elements [7] oscillatory blowing/suction [8], wall oscillation [9], vibrating ribbons [10], and zero-mass-flux, finite momentum actuators or synthetic jet actuators [11,12,13,14,15].

Suction from the surface of an airfoil has been used to remove low energy fluid directly from the boundary layer. This work was begun by Prandtl [4] and has been investigated successfully many times since by Kruger [5]. Along with suction of the boundary layer, introducing momentum via blowing has been used to energize the low energy region. High pressure air taken from an engine compressor has been used as the source for this momentum. Goodmanson and Gratzer [16,17] have shown in previous studies how these devices have been used. A jet has been used to blow normal to the flow and enhance the mixing layer [6,18]. The jet can be blown tangentially along a curved surface to take advantage of a phenomenon known as the "Coanda Effect". The tangential jet will contain a pressure gradient normal to the airfoil surface which helps overcome the adverse pressure gradient of a stalled flow. The pressure gradients that hold the emanating jet to a surface can also be exploited to obtain an increase in circulation. This is highly desirable as the lift is proportional to the amount of circulation around a body.

Recently, the synthetic jet actuator has been studied quite extensively in the areas of enhancement of mixing flows, separation control, wing shaping, and fluidic thrust vectoring. Most existing synthetic jet actuators utilized a small scale low-energy actuation to create micro disturbances into highly receptive regions of a flowfield. The disturbances into these regions create changes in the evolution of the fluid flow. Streamwise vortical structures are created from the small disturbances and energize the boundary layer. Seifert and Pack [13] have demonstrated that in order to gain the desired results from a synthetic jet actuator, there must be one to four vortices produced over the airfoil surface at any given time. Seifert has also shown that the most efficient excitation corresponds to the SJA being oscillated at an optimal non-dimensional frequency. The optimal non dimensional frequency is about one and is derived from the Strouhal number. The non-dimensional frequency is defined to be:

$$F^{+} = \frac{f \cdot c}{U_{\infty}} \qquad (1.1)$$

Here f represents the frequency of actuation; c is a reference chord length (usually the chord of the airfoil) and U_{∞} indicates the freastream velocity.

Many of the synthetic jet actuators used in preexisting technical literature have relied on systems that are driven piezoelectrically [19,20] or by external hardware [12,21,22]. This external hardware required for acoustic or pneumatic systems rest mainly outside of the test section of the wind tunnel. Applications typically require that the synthetic jets be small and compact so as to fit inside the control surface of the aircraft the performance of which they were attempting to modify. Although piezoelectric actuators have been light and compact they display poor performance characteristics away from actuator resonance frequencies and the maximum available amplitude is limited. The need for large amplitude was driven by the need to perform at higher Reynolds or Mach numbers. In previous research by Gilarranz and Rediniotis [14], a compact, high-power synthetic jet actuator was developed to meet the demands for size, weight, efficiency and power density needed for full-scale flow control applications. The creation and more in-depth description of the synthetic jet actuator can be found in Gilarranz and Rediniotis [14] and Gilarranz et al. [15]. This actuator was advantageous over piezo type actuators due to: its ability to achieve oscillation amplitudes of at least an order of magnitude higher, decoupling of oscillation amplitude and frequency, greater power density, smaller driving voltages, off the shelf construction materials [15]. The use of a synthetic jet actuator to reattach a separated flow field is shown in figures 1.1a and 1.1b. In figure 1.1a it can clearly be seen that without actuation the smoke traveled off the surface of the airfoil. With a leading edge synthetic actuator (figure 1.1) in use the smoke conformed to the surface and the separated region was eliminated.

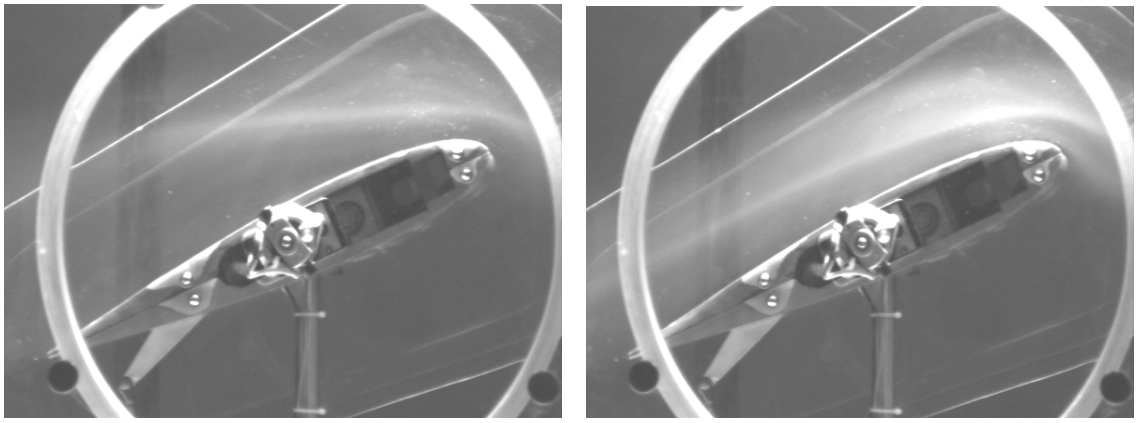

Figures 1.1. NACA0015 In a Flowfield, Without (Left) and With (Right) SJA Actuation.

This study focuses on using the flow mechanics of synthetic jet actuators for static and dynamic cases. A stalled aircraft creates a pronounced negative pitching moment brought about by the lack of pressure recovery over the aft section of the airfoil. In this high angle of attack region the synthetic jet can control the extent of flow separation and the center of pressure, thus generating moments. The dynamic pitching of a wing is shown to push the static stall angle beyond the normal stall giving greater area of control. The control of flow separation is achieved by using a synthetic jet near the leading edge of an airfoil. This is useful in the application where the angle of attack is at or near the region of stall. Although this application is demonstrated for pitch control at these high angles of attack [23], this mechanism is not operational at low angles of attack. The changes in the steady lift and moment coefficients, using a leading edge synthetic jet actuator, will be displayed in the leading edge synthetic jet actuator section. The importance of this feature is that the aerodynamic coefficients are varied continuously. The stall angle cannot be increased beyond a threshold of 25 degrees, and the leading edge synthetic jet had no effect below 16 degrees. The lack of control below 16 degrees angle of attack is due to the flow over the surface of the wing being completely attached. This lack of control has necessitated the need for actuation at locations other than the leading edge.

Traub et al. [23] showed that the synthetic jet was shown to be effective in slowing reattachment in dynamic cases and in affecting the creation of dynamic stall vortices. A sample of this data is shown in Figure 1.2 [24]. Here the wing underwent a sinusoidal pitching rate of 0.2 Hertz, through a range of zero to 20 degrees angle of attack. Significant effects to the coefficients of lift and moment were evident, especially concerning the reduction of hysteresis loops. It should be noted that for the greater portion of the pitching cycle (when the flow is attached) the synthetic jet had no effect.

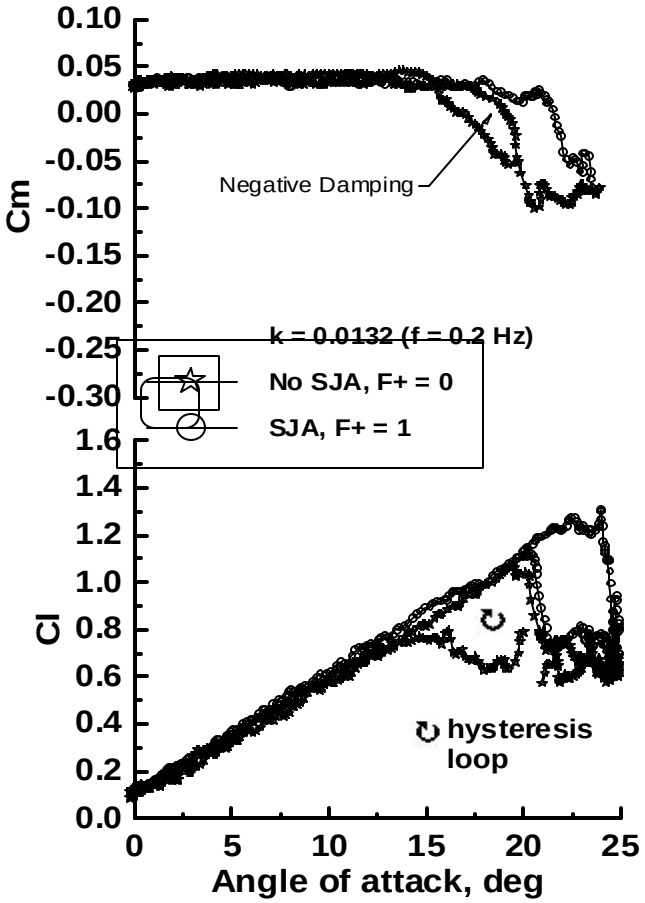

Figure 1.2. 0.2 Hz Sinusoidal Pitching of NACA0015

Trailing Edge Devices

To control the aerodynamic characteristics of the airfoil at low angles of attack, trailing edge devices were investigated. In an attempt to find a "hinge-less" form of control the Gurney flap was investigated. The Gurney flap is a very small trailing edge flap mounted perpendicular to the pressure surface of the airfoil surface. The usual application of the Gurney flap is shown in figure 1.3. This small flap greatly enhances the lift and pitching moment even though it is only 2% or less of the chord length [25,26,27,28]. The small flap was found to increase the camber of the wing in the vicinity of the trailing edge. Jeffrey et al [28] implemented a variety of testing and flow visualization techniques to show that the flap created increased loading across the chord of the airfoil. Also, a violation of the Kutta condition at the trailing edge was found. This violation of the Kutta condition in essence causes a pressure difference at the trailing edge. According to Jeffrey et al [28] it is this pressure differential that causes the increased loading over the airfoil. Jeffrey et al [28] shows that the adverse pressure gradient decreased resulting in an extension of the lift curve slope. The drag increased slightly with the introduction of a Gurney flap. Some of the data presented by Jeffrey et al [28] indicates that downsteam of the flap two counter rotating vortices formed. These vortices are non-stationary and equated to a von Karman vortex street.

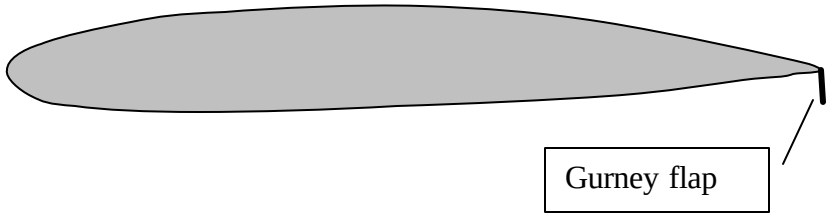

Fig. 1.3 Typical Gurney Flap Installation.

One of the advantages of the Gurney flap is that it is small and simple to implement. Experimental results of Gurney flap test have shown the effectiveness of these devices [29]. The desire for “hinge-less” control necessitated the development of a flow device that mimics the Gurney flap. This need has led to the testing of continuous jets at the trailing edge of an airfoil to create aerodynamic effects. The comparison of these tests can be found in Traub et al [30]. The study shows that a jet in the trailing edge created large enough lift and pitching moment changes to facilitate control. This data also shows that unlike the Gurney flap the continuous jet displayed no zero angle of attack drag penalty [30].

It was decided that a trailing edge synthetic jet actuator would be used instead of a continuous jet. This decision was based on the need to have a self contained method of generating jets of air. The synthetic jet does not require bleeding air from a compressor or onboard compressed air tanks. In the case of remote control aerial vehicles, electrical power will be available although compressed air will not. It will be shown that the synthetic jet can be effectively used as a trailing edge flap substitution.

2. WIND TUNNEL TEST FACILITIES

Tests were undertaken at a freestream velocity, U, of 20m/s yielding a Reynolds Number of $0.57x10^6$. The tests were undertaken in Texas A&M University's 3' by 4' closed loop wind tunnel. The free stream velocity was measured using a Pitot static tube (differential pressure measurement). A differential pressure manometer was used to measure the pressure form the Pitot tube and a corresponding velocity was found assuming incompressible flow. The tunnel temperature is maintained constant throughout testing periods by a cooling unit installed in the tunnel.

Tunnel turbulence intensity was measured (using a hot wire anemometer system) at less than 0.5% assuming isotropic turbulence. Data acquisition was facilitated using a 3-component Pyramidal balance. Conditioned and amplified balance output voltages were read using a 16-bit A/D board. A dedicated software acquisition code was written for this facility and used for acquisition and processing. Prior to use for these experiments, the Pyramidal balance was re-calibrated. Subsequent balance verification through application of pure and combined loads suggests accuracies better then 0.6% for lift, drag and pitching moment. Wind tunnel corrections for solid and wake blockage were applied using the methodology described in Rae and Pope [31].

3. LEADING EDGE SYNTHETIC JET ACTUATOR

General

This section presents the effects that a leading edge synthetic jet actuator has upon the aerodynamic characteristics of an airfoil. The methods used to build and test the model are discussed.

Leading Edge Wing Design and Fabrication

The wing profile for the leading edge synthetic jet actuator test is a NACA 0015 airfoil. This shape was chosen due to the ease with which the wing could be manufactured and the available interior space for accommodating the synthetic jet actuator (SJA). The wing chord length is 420 millimeters with a span of 430 millimeters. The exterior structure of the wing comprises of three separate pieces: the upper and lower surfaces and the trailing edge section. The lower portion of the wing was fabricated from a solid piece of Aluminum. The lower section was designed to hold the SJA, and was mounted to the sting by means of two bearings. The lower section contains an inbuilt firewall to protect an ESP Pressure Scanner from thermal effects. This section also took the bulk of the forces created from the pitching of the wing. This lower wing half was machined out of a solid 0.45-meter x 0.45-meter x 0.038-meter plate of aluminum. This metal plate was machined using the Bridgeport CNC mill of the Department of Aerospace at Texas A&M University. Figure 3.1 shows the inside view of the lower wing section. From this view the different compartments for the SJA and the ESP can be seen. Also, a small channel that was created to accommodate pressure tubing from tapping holes on the surface to the ESP is shown. Figure 3.2 shows a closer view of the ESP, the firewall, the channel for the routing of the pressure tubing and the rear section of the wing. Figure 3.3 shows a picture of the outside surface of the lower (aluminum) wing panel. In this figure the holes for the sting, mounting and pressure tappings can be seen.

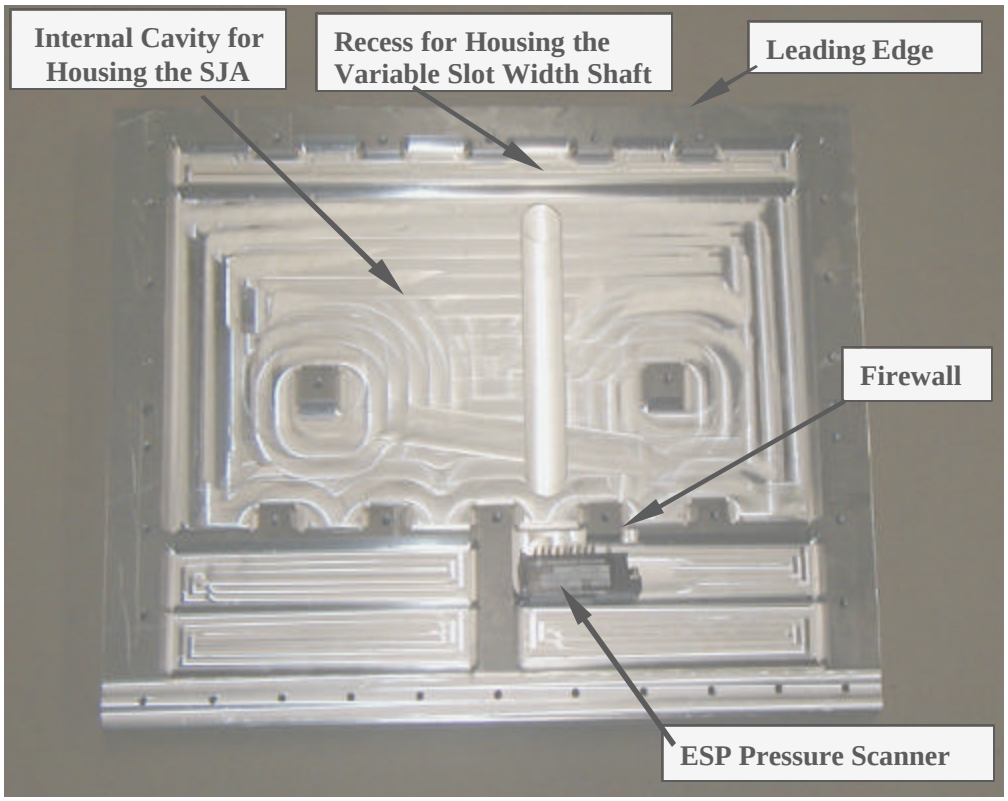

Figure 3.1. Lower Wing Panel of the Leading Edge Model.

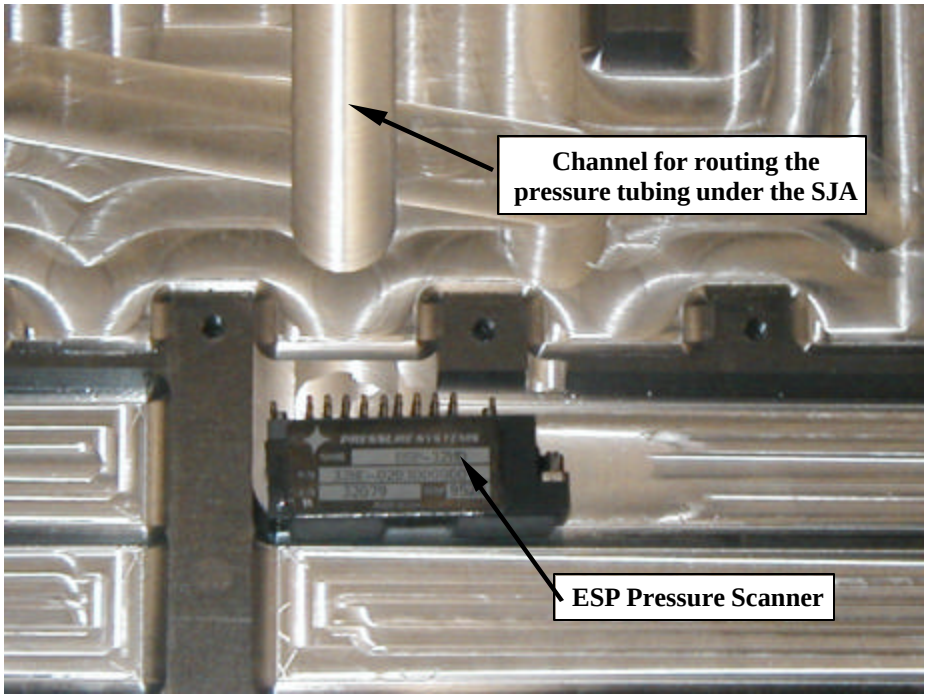

Figure 3.2. Structural Details of the Lower Wing Panel of the Leading Edge Model

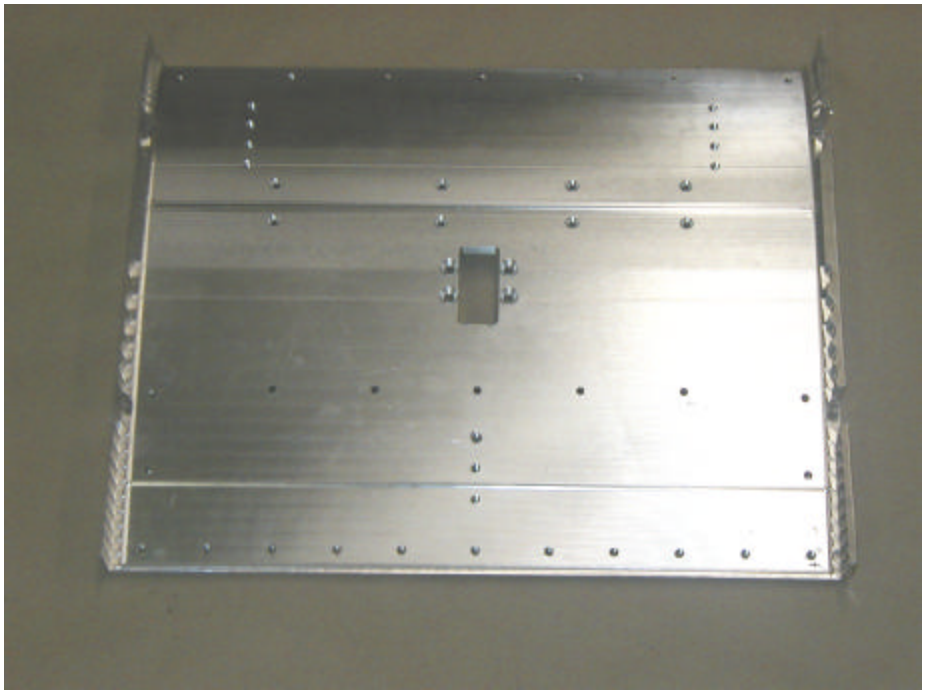

Figure 3.3. Outside Surface of the Lower Wing Panel of the Leading Edge Model

The second structural component of the wing was the upper portion made of a single piece of Plexiglas®. Plexiglas® was chosen since it is a transparent acrylic that allows for visibility of the inner components of the model. This was useful in determining if any tubing has been pinched or wires have become disconnected. Figure 3.4 illustrates a solid model of the inside of the upper surface of the wing. The large opening in the upper surface to accommodate the plenum and SJA exit slot chamber is shown. The different compartments can be seen. The upper portion of the wing has also been machined from a solid piece of material using the Bridgeport CNC mill. Figure 3.5 shows a picture of the finished outside surface of the upper (Plexiglas®) wing panel, mounted in the CNC machine.

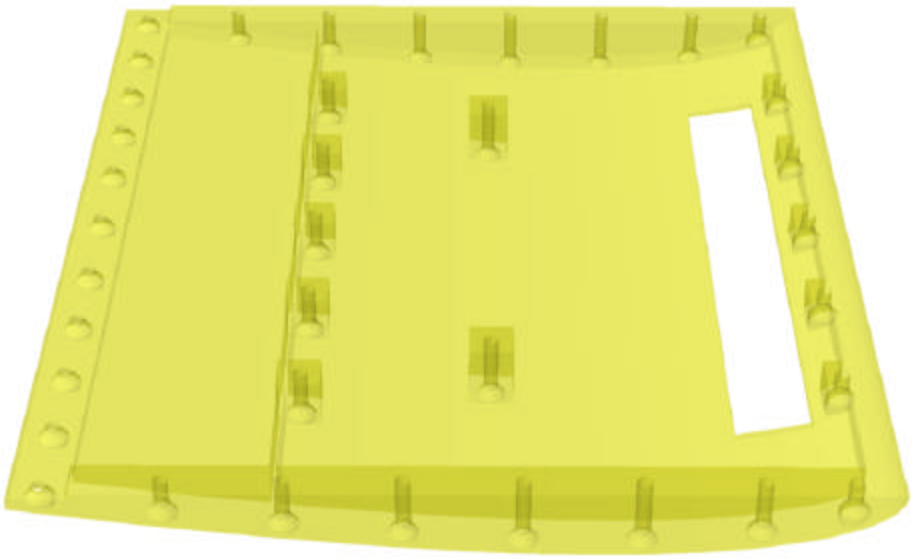

Figure 3.4. Upper Wing Panel of the Leading Edge Model

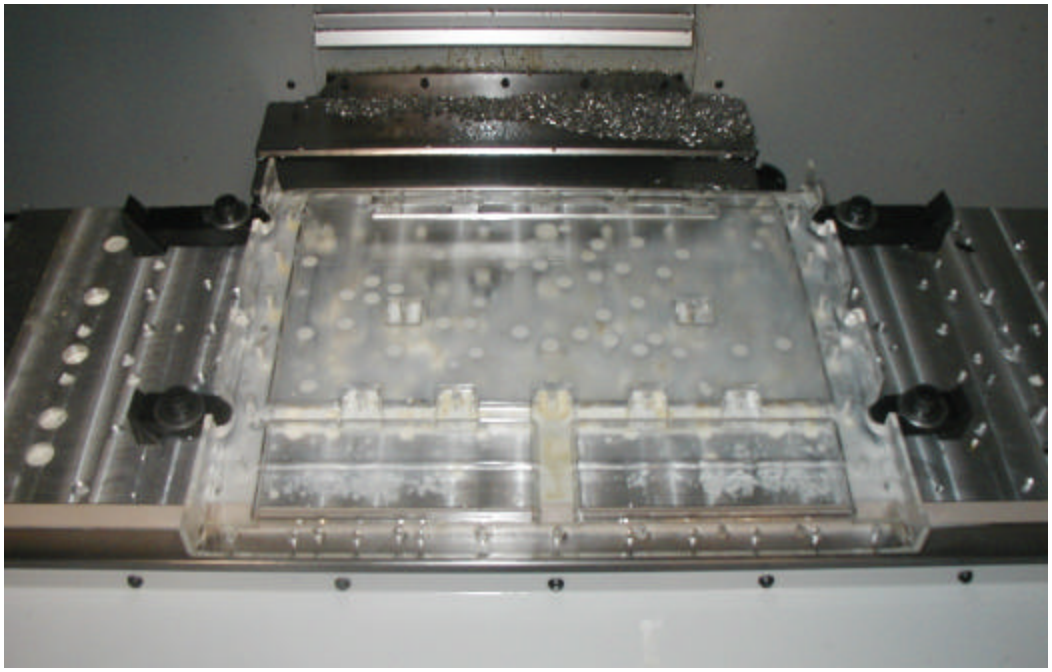

Figure 3.5. Upper Wing Panel of the Leading Edge Model

The third component of the structure was the trailing edge of the model. This section was created using our Rapid Prototyping Machine, and was consequently manufactured from ABS plastic. The three exterior sections of the model can be seen in Figure 3.6. Figure 3.7 shows how the piston driven SJA and plenum exit slot were located inside the wing. Figure 3.8 is a picture of the piston driven synthetic jet and wind tunnel model mounted inside of the 3' x 4' wind tunnel. The interior of the model contained: housing mounts for the sting, the SJA, the variable exit slot plenum at 12% chord location, and the ESP. The ESP is further discussed in the Leading Edge Wing Experimental Setup portion of this section.

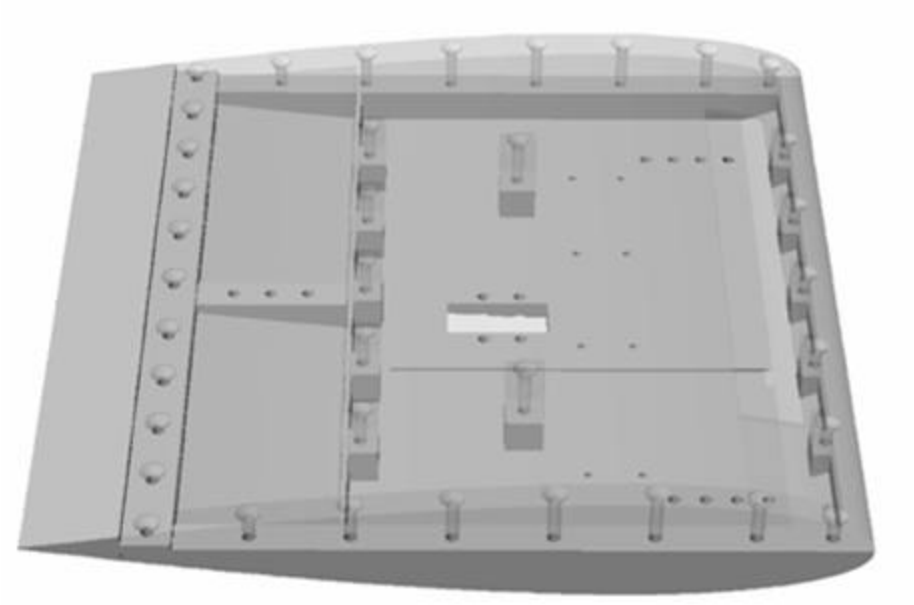

Figure 3.6. Leading Edge Wind Tunnel Model Without SJA

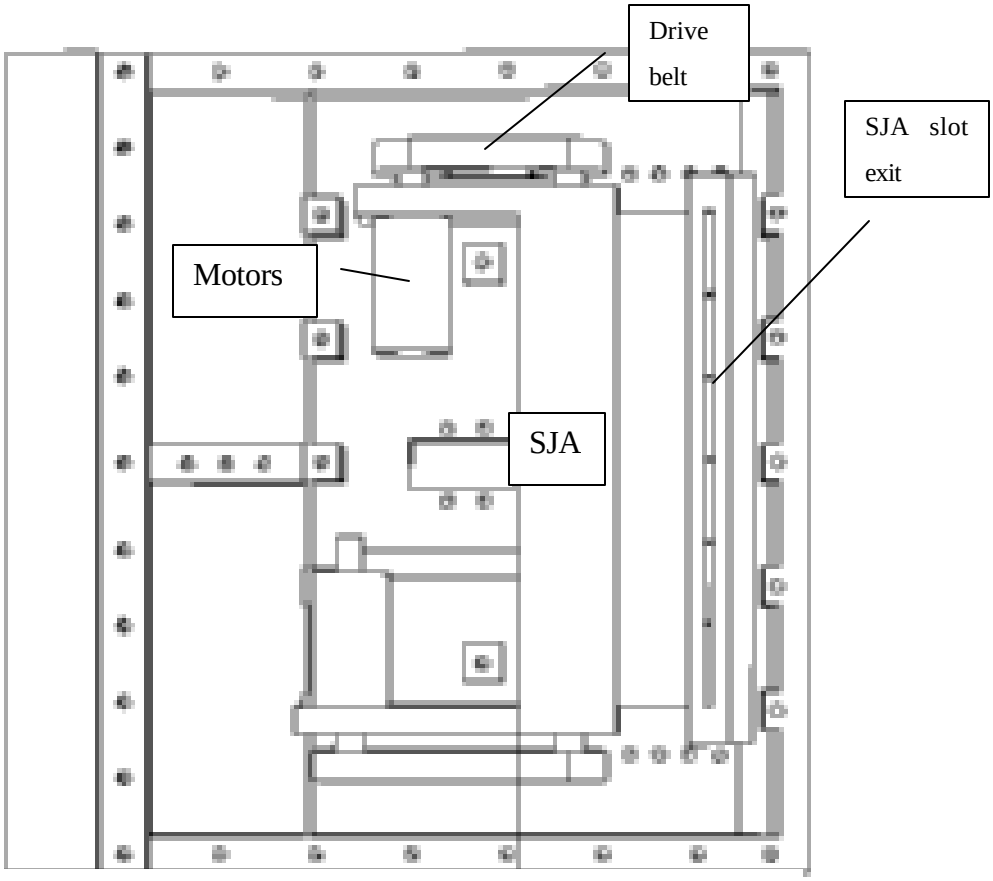

Figure 3.7. Placement of SJA Inside the Leading Edge Model

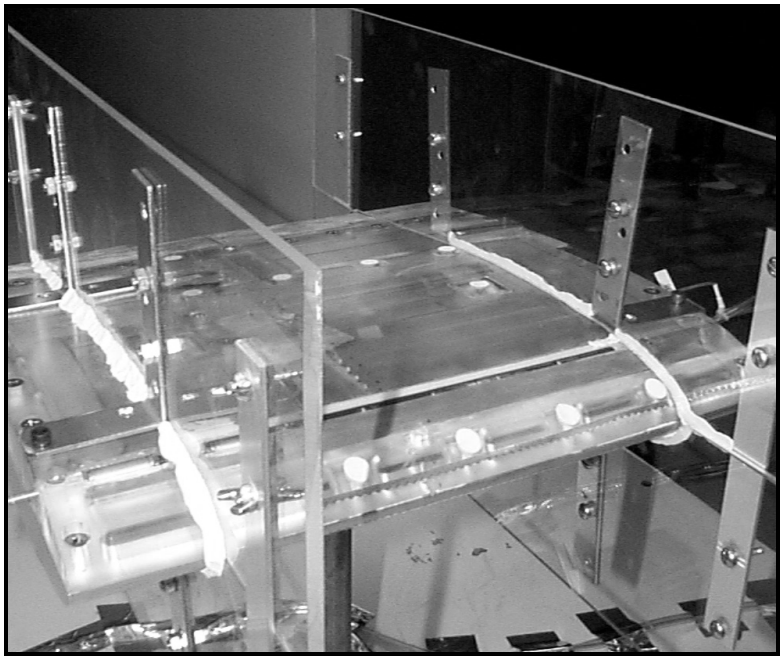

Figure 3.8. Leading Edge Model Mounted Inside the Wind Tunnel

Characterization of Leading Edge SJA

The behavior of the leading edge synthetic edge actuator was studied to evaluate its performance. These studies consisted of measurements that are performed using a TSI model 1054 hot wire anemometer. The location of the position of the hot wire sensor is shown in the inset of Figure 3.9. The hotwire can be seen to be placed just at the entrance of the jet. The stability and damping of the anemometer were adjusted to maximize the frequency response of the equipment, prior to testing, for the highest expected velocity. The method of calibration used for the hot wire was a quadratic relation of a known air velocity to a measured bridge voltage.

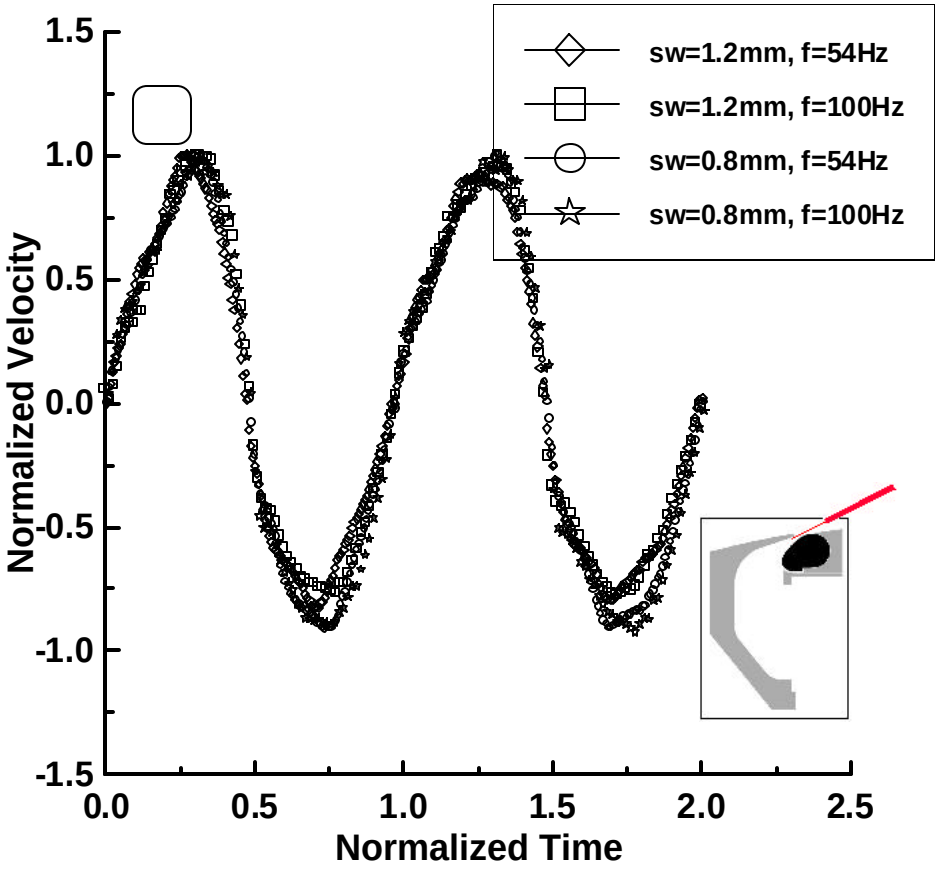

Figure 3.9. Normalized Velocity of Synthetic Jet

The known air velocity for the hot wire calibration was supplied using a TSI calibration unit. The results were de-rectified to display the correct direction of magnitude of the velocity. The normalized velocity produced during each cycle is displayed in Figure 3.9. This data is normalized to show the sinusoidal nature for different slot widths and synthetic jet actuation speeds. It can be seen that, at the exit of the synthetic jet, the normalized velocities are quite similar. The compressibility of the piston driven synthetic jet with the plenum of the leading edge was investigated. The results of this study are shown in Figure 3.10. The parameter K (determined from the Continuity equation) should be a constant for a given piston and stroke combination if the fluid behaves as incompressible.

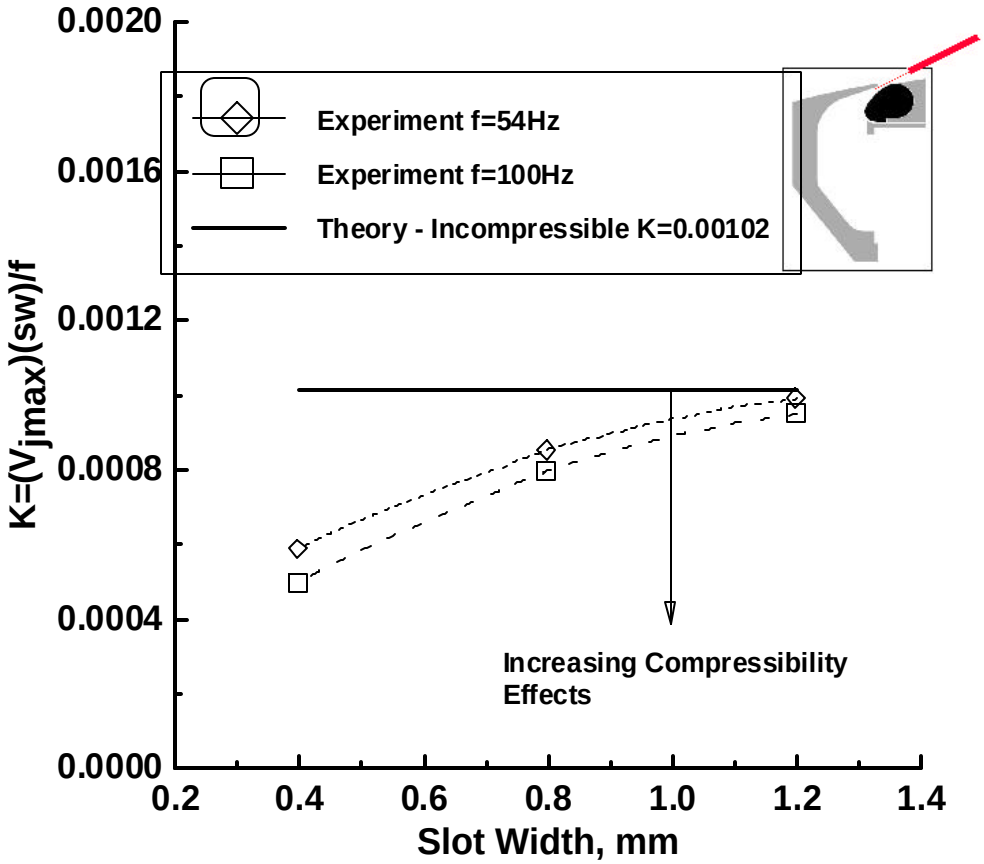

Figure 3.10. Effect of Slot Width and Frequency on Compressibility

The derivation of the parameter *K* is shown below.

$$r_{piston} \cdot Area_{piston} \cdot v_{piston} = r_{exit} \cdot Area_{exit} \cdot v_{exit} \qquad (3.1)$$

Assuming that the flow is incompressible then $r_{piston} = r_{exit}$

$$Area_{exit} = sw \cdot l$$

$$Area_{piston} \cdot v_{piston} = f \cdot Volume_{piston}$$

Therefore, $K = \frac{Volume_{piston}}{l} = \frac{sw \cdot v_{exit}}{f}$ (3.2)

The results of the testing indicated that around a slot width of 1.2mm and above the flow can be assumed to be incompressible. Reducing the slot width caused a significant increase in the effects due to compressibility. Figure 3.10 also reiterates that as the

frequency of the actuation was increased, from 54 Hertz to 100 Hertz, the losses due to compressibility increased. SJA performance, quantified in terms of exit velocity, is presented in figure 3.11.

For a 1.2mm slot exit, the exit velocity was seen to vary essentially linearly with actuator frequency, reflecting the marginal effect of compressibility for this geometry. The maximum velocity measured at the slot exit is also indicated for slot widths of 0.4 and 0.8mm. Although the sparse nature of the data mitigates establishment of characteristic trends, the form of the data suggests a somewhat linear dependence of velocity on frequency in this range. Maximum jet exit velocity as a function of slot exit width for two driving frequencies is detailed in figure 3.11. Reducing the slot exit width increased jet exit velocity; however, compressibility effects lessened the relative increase in velocity. Nonetheless, for a 0.4mm slot exit, a jet exit velocity of 124m/s (peak) was recorded (f=100Hz).

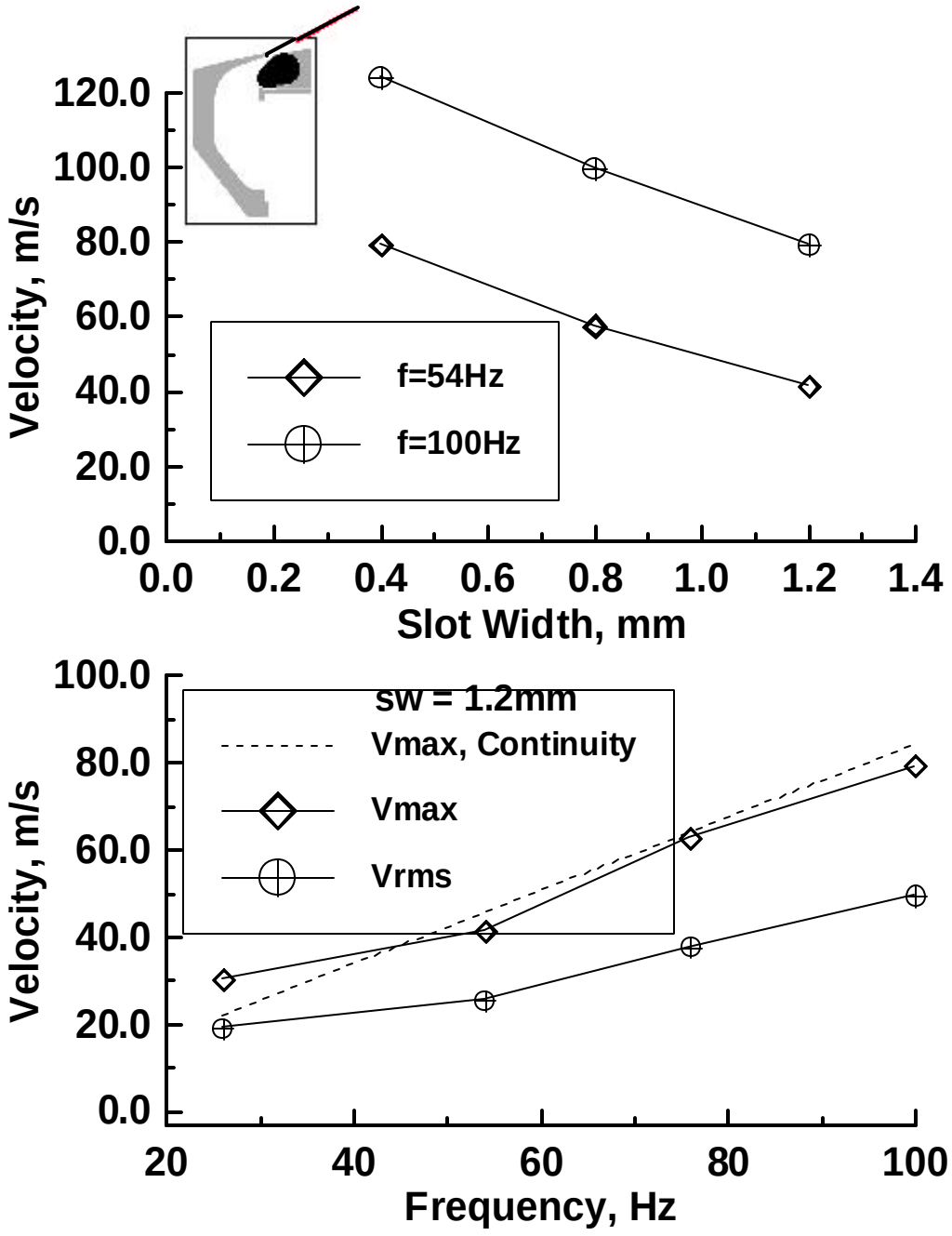

Figure 3.11. Effect of Slot Width and Frequency on Velocity of Jet

Leading Edge Wing Experimental Setup

To quantify the effect of the leading edge synthetic jet actuator upon the wind tunnel model the aerodynamic characteristics (change of the coefficient of lift and coefficient of moment) were measured. Surface pressure measurements were used to measure the resultant moment and lift. A 32-channel ESP pressure scanner was inserted in the wing as seen in Figures 3.1. and 3.2. The transducers that comprised the ESP have ranges of $\pm 10 in H_2O$ ($\pm 2.49 kPa$). Prior to use, the ESP was calibrated using an Edwards's Barocel as a reference. The locations of the pressure port tappings on the wind tunnel model are denoted in Figure 3.12.

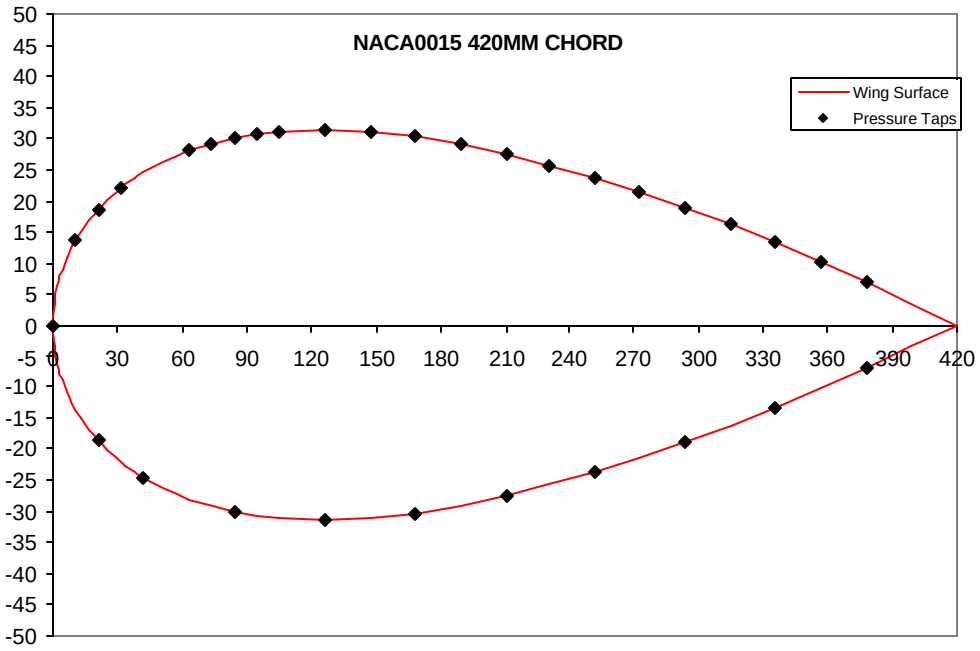

Figure 3.12. Locations of Pressure Tappings on the Leading Edge Model

The surface pressure ports are connected to the ESP using 16" long, 0.02" inside diameter, microbore Tygon® tubing. The tubing internal diameter was selected following frequency response analysis related to the acoustic lag that will be discussed shortly. For the dynamic portion of the experimental work the acoustic effects on the

pressure sensing equipment needed to be determined. The acoustic effects were governed by the geometric parameters of the system. A pre-existing acoustic test facility developed by Johansen [32] was used to determine the transfer function associated with the dynamic behavior of the tubing and ESP. The findings of the testing showed that the tubing and ESP pressure scanner created an over-damped system. Figure 3.13 shows that the ratio of the sensed pressure magnitude over the true pressure magnitude was about 99 percent in the lower frequency ranges and decreased as the frequency increased. An over-damped system was necessary to implement a simplified method for rectification for lag effects created by Wildhack [33]. This method is unusable if the system should be under-damped. The governing equation for the correction of the pressure is

$$p_s = p_r + l\frac{\partial p}{\partial t} \quad . \tag{3.3}$$

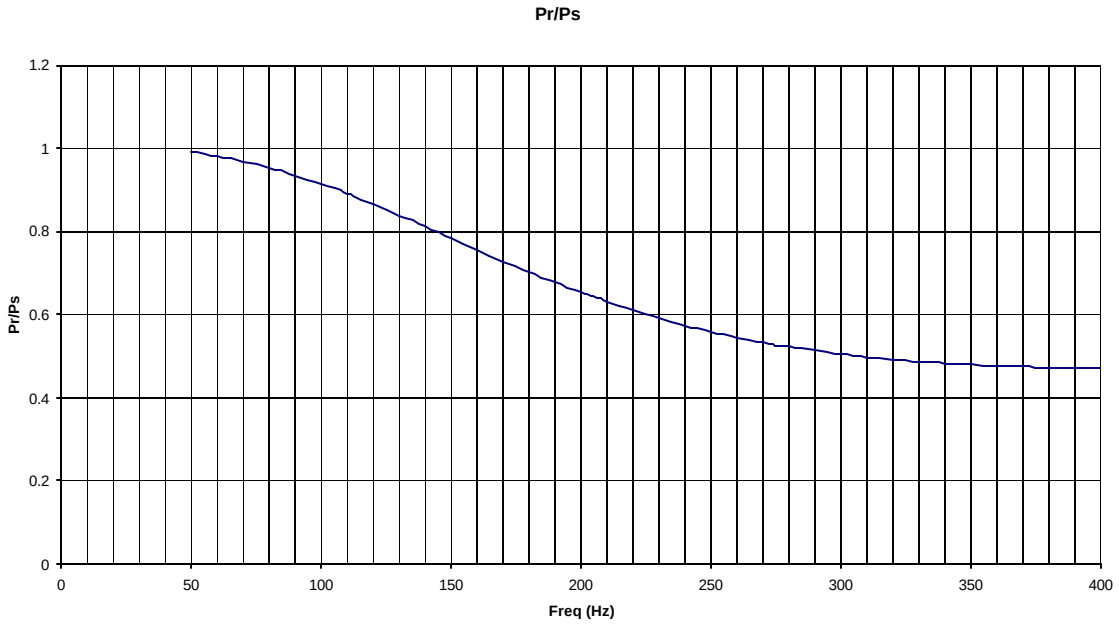

Figure 3.13. Unsteady Pressure Excitation Tests of ESP and Tygon Tubing

The ? parameter in the above equation can be found experimentally or estimated using the method from Wildhack [33]. For the purposes of this study the ? parameter was calculated experimentally. Using the corrected pressure readings the lift and moment were calculated through the integration of the pressure distribution. Cubic splines were fitted to the upper and lower surface pressure traces. These cubic splines were then integrated. The moment was calculated about the quarter chord. The locations of the pressure taps are shown in figure 3.12.

Figure 3.8 shows the wind tunnel model containing the leading edge synthetic jet actuator mounted into the test section. In the picture the side plates on the wing can be seen. The side plates were added onto the model to ensure quasi-two-dimensional behavior of the flow field.

The leading edge synthetic jet wind tunnel dynamic model was supported by a vertical strut attached to the wing by internal bearings. The pitching motion for the dynamic test was accomplished using a stepper motor produced by SLO-SYN® . The stepper motor is capable of a torque of 5 Newton meters and is controlled by a microLYNX® 4/7 micro stepping motor controller. The stepper motor has 200 steps per revolution, wherein the micro*LYNX*® allowed micro stepping up to 51,200 steps per revolution. The micro*LYNX*® motor drive allows control over motor acceleration, initial velocity, maximum velocity, slew rate etc. Consequently, the motor drive allows the wing to be accurately pitched at a constant angular velocity. The attachment of the stepper motor to drive the movement of the model was accomplished using a strut attached to the trailing edge of the wing. Figure 3.14 illustrates the model setup used for the dynamic pitching experiments. The stepper motor was connected via a linkage to a pitch strut. The SJA exit slot width was also controlled using a stepper motor (VEXTA Model PXB44H-02AA-C1) with 200 steps/revolution. A second micro*LYNX*® 4/7 micro stepping motor drive was used to control this motor. The ESP pressure scanner data was digitized using a 16-bit Computer Boards A/D board. For each of the data sets thirty ensemble averages

were acquired. The angle of attack of the wind tunnel model during the dynamic test was measured using an encoder mounted to the shaft of the driving stepper motor. The data acquisition was accomplished via a dedicated program written in BASIC. The program not only recorded all of the data but also controlled the stepper motors for pitching and slot width control.

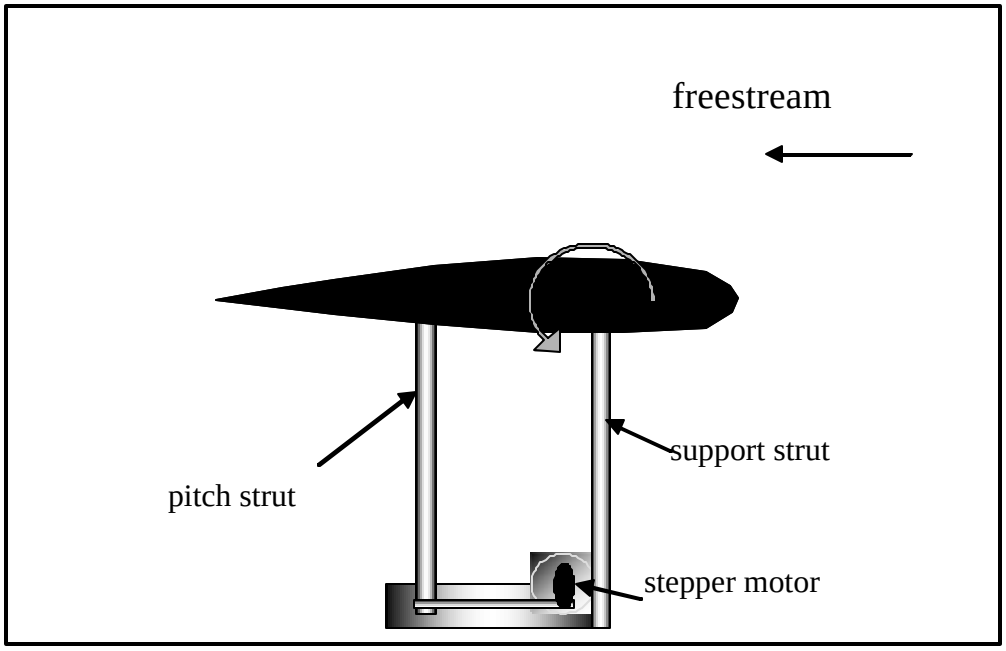

Fig 3.14 Diagram of Experimental Setup of Pitching Wing

To test the wind tunnel model and data acquisition system a validation experiment was carried out. The model was introduced in a freestream velocity of 20 m/sec and was fixed at an angle of attack of 10 degrees. The pressure coefficient distribution was experimentally measured. The pressure coefficient distribution was also theoretically calculated using a Smith Hess Panel Method. The comparison for the two cases is shown in figure 3.15. This displays the validation of the setup and the data acquisition processes

.

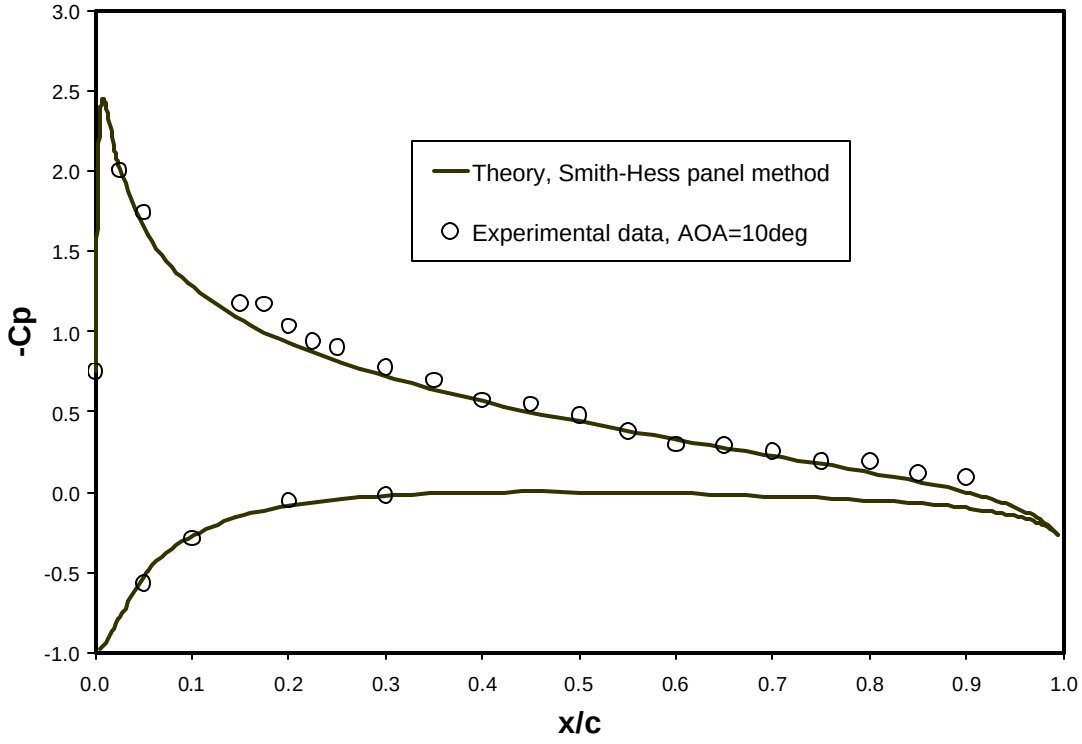

Figure 3.15. Smith-Hess Panel Method vs. Experimental Results.

Static Leading Edge Wing Results

The first tests undertaken utilizing the leading edge synthetic jet were the static wind tunnel tests. The majority of these tests focused heavily on the resultant moment coefficient produced from the synthetic jet actuation. The SJA was driven at frequencies from 0 to 100 Hz. The non-dimensional frequencies (F^+) used were between 0 and 2. The slot width varied from 0.4 to 1.2 millimeters. The resulting coefficient of blowing (C_μ) was between 0.0023 and 0.019. It was found that both C_μ and F^+ were the driving parameters of the actuator mechanism in the flow field. Studies suggested that the global synthetic jet effectiveness was weakly affected by F^+ in the range of $0.5 < F^+ < 1.5$ [8,34]. This F^+ range also (approximately) corresponds with Seifert and Pack [21] to that which has been generally accepted as optimal for fluidic actuation. The effect of C_μ was the more important of the two parameters. Without an adequate level of C_μ, flow

control is unattainable [2]. It should also be noted that at high levels of C_μ, flow control can be established despite being outside of the optimal ranges of F^+ according to Chang et al [2]. At high levels of C_μ the lift and moment coefficients become independent of the jet-momentum coefficient. For the data presented in this study C_μ and F^+ were coupled and the F^+ values were inside their optimal range. The aerodynamic characteristics are evaluated as functions of the jet-momentum coefficient. Figure 3.16 shows the coefficient of lift for one of the static tests conducted with the leading edge synthetic jet model. Here the effect of the SJA on the separation point of the wing was clearly visible by the extension of the lift curve. It should be noted as well that the lift was controlled throughout the range from 17 – 25 degrees angle of attack. The enhancement of lift is achieved by reattaching the flow to the surface of the wing. Figure 3.17 displays the coefficient of moment data taken during a steady state test using the same leading edge synthetic jet. As with the lift of the wing, the moment was changed by manipulation of the separation point. Also, as with the lift the amount of moment on the wing was controlled though the 17 – 25 degree angle of attack range.

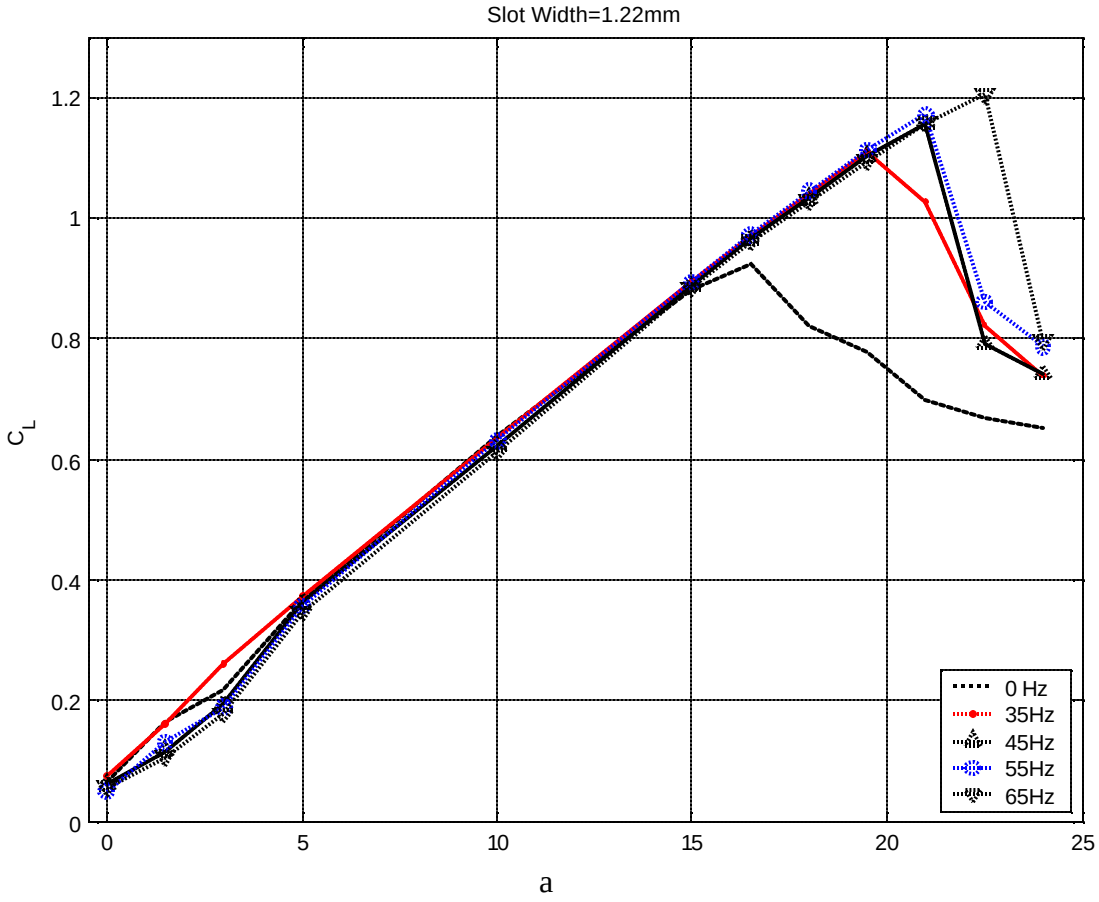

Figure 3.16. Effect of Leading Edge SJA Upon Coefficient of Lift

A flow survey using a TSI hot-wire anemometer over the wing upper surface was undertaken to better understand the nature of the physics that is involved in a leading edge synthetic jet actuator. The hot-wire was placed at an axial location of 32% of the chord, at its closest-to-the-leading-edge location. For this analysis the wing was fixed at an incidence of 20 degrees angle of attack. The hot wire was traversed perpendicularly to the airfoil surface using cosine point spacing. In the Z_{normal} direction this consisted of 25 points. At each of the locations approximately 8000 readings were collected at a speed of 8 kHz. The temporal phasing of the data was achieved via a Hall Effect sensor attached to the synthetic jet motor shaft. The data was then phase averaged. Figure 3.18 illustrates the normalized flow velocity at the locations mentioned above. The eight

plots show the instantaneous phase-averaged velocity profiles at successive time instances in the flow through one cycle of the synthetic jet. From the figure, it can be seen that the synthetic jet actuation caused direct boundary-layer injection of momentum. In the middle of the cycle, t=0.5T, the boundary-layer is "full" and appears to be fairly even. In contrast, at the beginning and end of the cycle the usual boundary-layer profile can be observed. Also note that no apparent "jetting" in the near surface boundary layer is evident in Figure 3.18. This shows the rapid attenuation of the jet caused by viscosity and spreading.

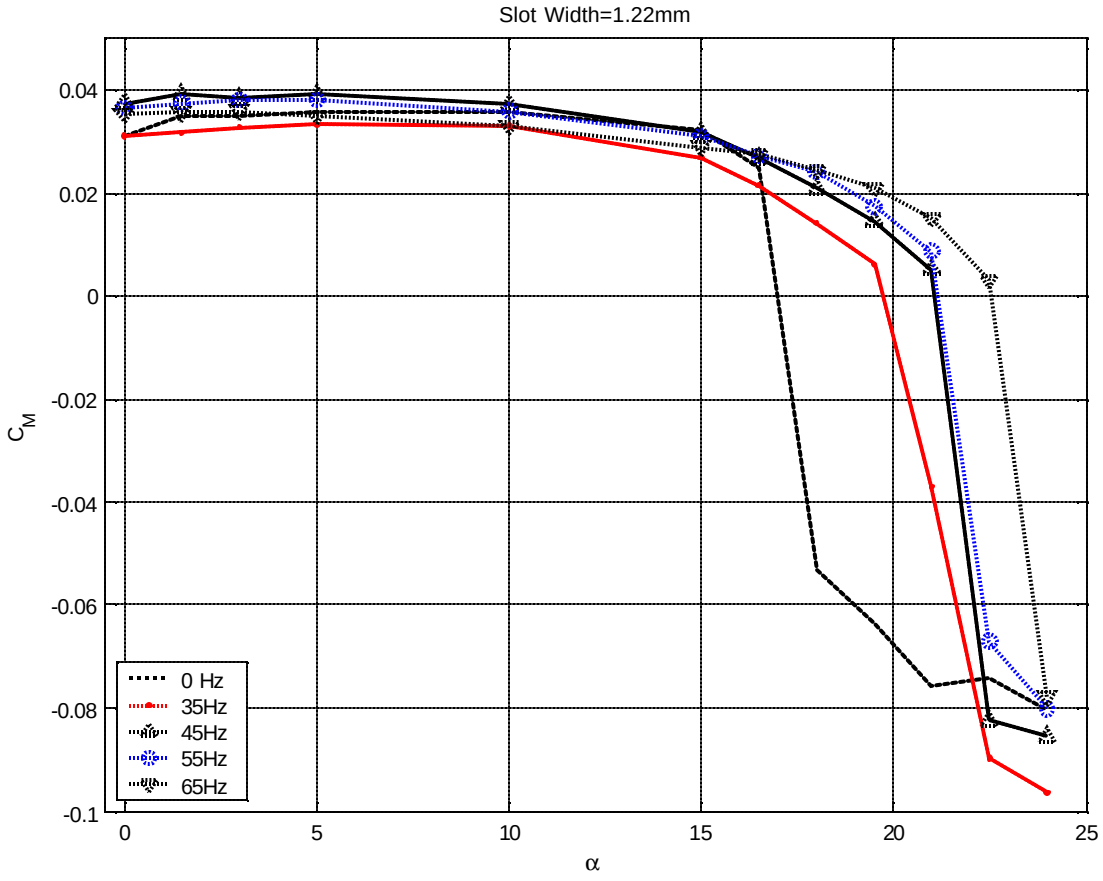

Figure 3.17. Effect of Leading Edge SJA Upon Coefficient of Pitching Moment

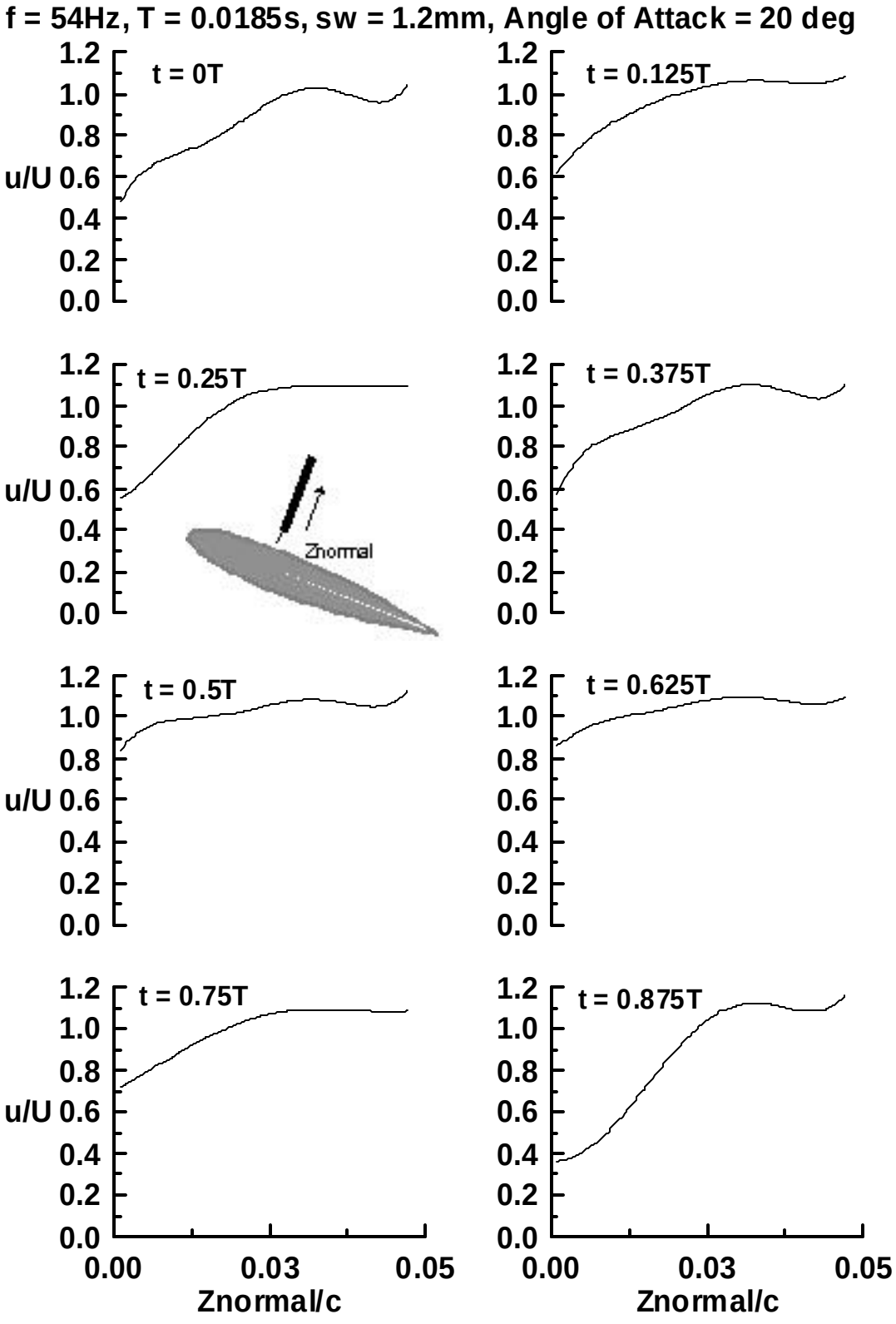

Figure 3.18. Instantaneous Velocity Profiles Over the Leading Edge Model

Dynamic Leading Edge Wing Results

The next phase of experimentation was conducted while pitching the leading edge synthetic jet actuator model. The first test consisted of the wing being pitched from 0 to 27 degrees at differing pitch rates and differing settings of the synthetic jet. The angular pitch rate during each of the tests was constant throughout the pitch motion. Since the synthetic jet actuator frequency was much larger than the model angular pitch rate, a phase relationship was unnecessary [12]. The slot width was set prior to the pitching motion and remained constant throughout the duration of each test.

All of the jet-momentum coefficients (C_μ) stayed within the effective range of values afforded by Lorber et al [35]. The jet-momentum coefficient indicated the momentum contained in the emanating jet. The effectiveness of the use of the jet momentum was determined from the amount of lift augmentation achieved. The RMS (root mean square) values used for the calculation process were determined using velocity time histories taken from the TSI hot-wire anemometer. The uncertainty of C_μ was estimated to be about 2%. Table 3.1 also contains V_{max}/U (the ratio of the jet velocity to the free stream velocity), which was also found from the hot-wire data. The data is presented such that the aerodynamic characteristics are evaluated with their dependence on the jet-momentum coefficient. The freestream velocity of the test was 20 m/sec unless otherwise noted. While the wing was undergoing its pitching motion, data from the 32 pressure ports were recorded. For each pitching motion approximately 130 sets of data were recorded. The same tests were conducted thirty times to ensemble average the data sets. The effects of the Reynolds number on the ramping motion were diminished using both natural and forced transition (accomplished via a trip strip) located at 5% of the root chord. The pressure data allowed for the estimation of regions of attached and separated flow or the presence of any coherent vortical structures. Integration of pressure data also gave the sectional loading. It should be noted that measurements of the lift curve yielded values of approximately 0.8p. This was believed to be an effect of the end plates

not causing truly two-dimensional flow. The three-dimensional effects were assumed to be insignificant due to the comparative nature of the experiments.

Table 3.1 Jet Momentum Coefficient Summary

sw, mm	C_μ	F+
0.4	0.013	1
0.6	0.012	1
0.8	0.013	1
1.2	0.009	1
1.2	0.019	1.4
1.2	0.0048	0.66
1.2	0.0023	0.33

Figure 3.19 presents the effects of the jet-momentum coefficient upon the lifting and pitching moment, integrated from the corrected pressure measurements. This data shows three cases where the slot width has been set at 1.2mm and the speed of the synthetic jet actuator was changed between the cases. The C_μ varies from 0 to 0.019. The jet-momentum value of zero corresponded to the case where the synthetic jet was not active. The airfoil was pitched linearly at a non-dimensional rate of 0.009. This corresponded to pitching the model 27 degrees in one second. An optimal F^+ value of about one was used to correspond with prior studies by Seifert et al [20] that suggested this is optimal since it indicates the presence of 2 to 4 convecting vortical structures above the upper surface.

The data also demonstrated that a dynamic stall vortex formed for all of the values of C_μ used. The dynamic stall vortex is important in this discussion since it is associated with a significant nose-down pitching moment because of the streamwise advection of the vortex and its associated induced localized loading. Fluidic actuation significantly

delayed the onset of the dynamic stall vortex formation by approximately 6 degrees of the angle of attack. The results also have shown that the rounding of the lift curve slope was reduced with the use of actuation. The rounding of the lift curve slope was an indicator of the trailing-edge boundary-layer thickening and flow separation. In addition the strength of the dynamic stall vortex appeared to be strengthened when compared with the cases that had no actuation. It is possible that this was a result of the synthetic jet actuator being able to effectively organize the separated shear layer into a coherent structure and keep it in a closer proximity to the surface of the airfoil. When the two test cases that involve actuation, C_μ=0.019 and C_μ=0.009, were evaluated, it was demonstrated that only a marginal change in the delay of the dynamic stall vortex was seen. This is more readily seen in the portion of the graph relating to the coefficient of moment. This suggests that the jet-momentum values were possibly large enough to reach saturation. It should be noted that a change in lift and pitching moment was achieved at large angles of attack with proper utilization of the leading edge synthetic jet actuator. These changes in the aerodynamic characteristics could be exploited for control at these large angles.

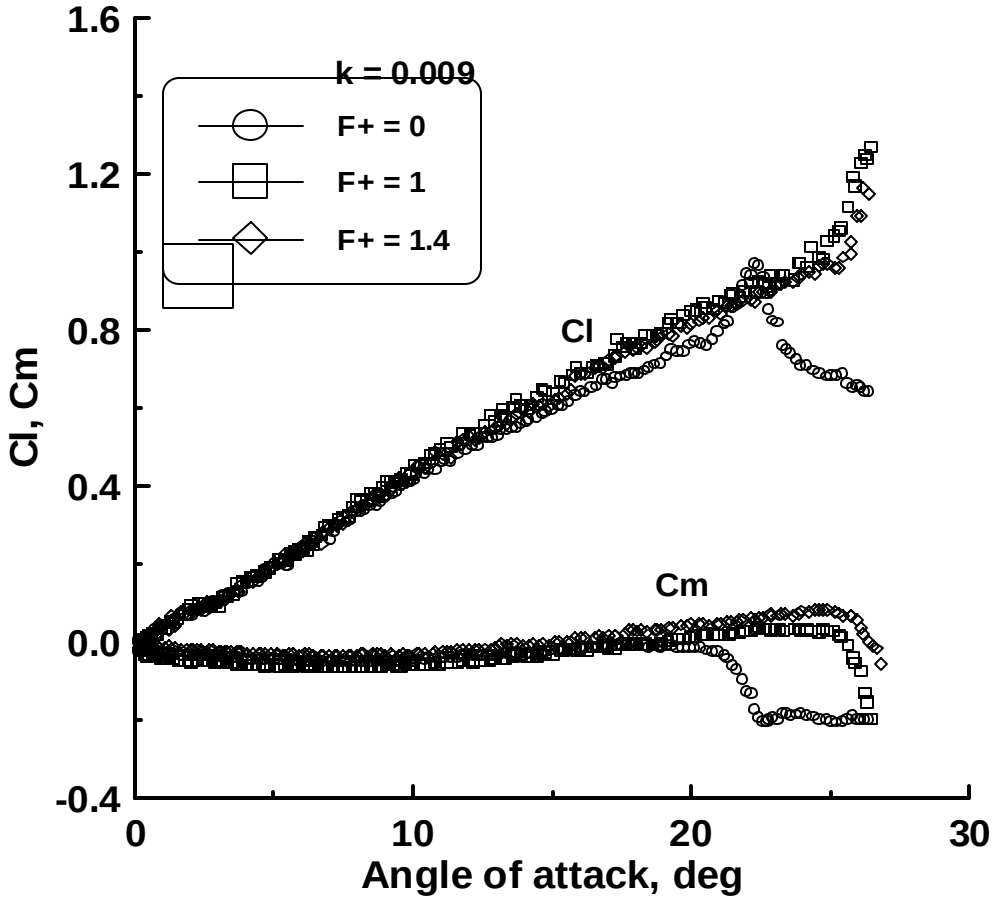

Figure 3.19. Lift and Moment Curve Slopes of Various SJA Speeds

Figure 3.20 shows the change in the dynamic stall vortex with systematic variations of the jet-momentum coefficient. In this range it is shown that as the jet-momentum coefficient increases the dynamic stall vortex formation is postponed. However it is noticed that the induced surface loading, due to the dynamic stall vortex, was larger, for the cases where C_μ=0.0023 and C_μ=0.0048, than in the case where C_μ=0.019, even though this corresponds to a four-fold increase in the jet-momentum coefficient. The induced surface loading was the difference between the peak loading and the loading at the beginning of the dynamic stall vortex. The lack of strength of the induced surface loading for the large jet-momentum value could have been a result of the time frame when the vortex forms. For example, in the cases of the two smaller values, the vortex formed before the completion of the pitching motion. Airfoil kinematics can thus cause

closer airfoil vortex spacing than for the case where C_μ=0.019, and the vortex inception occurred just before the pitch motion of the wing has ended. Another possible cause for the discrepancy could be because of the nature of the jet that was formed by the SJA.

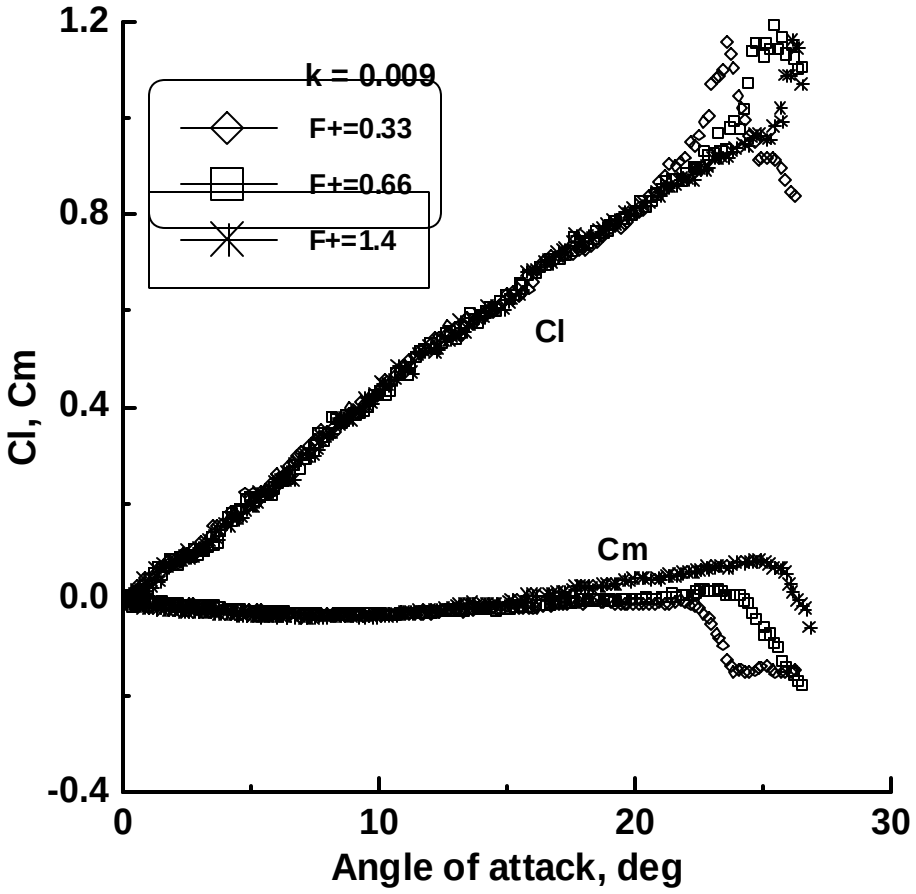

Figure 3.20. Lift and Moment Curve Slopes of Various SJA Speeds

For jet-momentum coefficients of 0.0023 and 0.0048 the jet velocity ratio was 1.5 and 1.7 respectively. This was approximately the same as the potential flow velocity adjacent to the airfoil surface aft of the synthetic jet. This would lead to the conclusion that the jet exit velocity and the potential flow yielded similar velocities. In the case where C_μ=0.019, the jet velocity ratio was approximately 3. The near-wall potential flow prediction was roughly 1.8. In essence this caused the synthetic jet actuator to form an oscillating overdriven wall jet. Consequently, the shear layer that formed the

dynamic stall vortex after the boundary-layer eruption/separation would contain vorticity of both signs, reducing the total circulation forming the dynamic stall vortex.

An instantaneous view of the pressure distribution along the upper surface of the airfoil at an angle of attack of 25 degrees was shown in figure 3.21. The flat pressure distribution in the case without actuation was an indicator that the flow was massively separated over the upper surface. For a jet-momentum coefficient of 0.0023, a similar result was noticed. This can be explained from figure 3.22. At an angle of 25 degrees, for this case, the dynamic stall vortex has traveled off the surface and the flow has separated. The other pressure distributions show the attached flow with leading edge suction peaks. The life-cycle of the upper surface distribution for the case with no actuation is displayed in figure 3.22. The dynamic stall vortex can be seen in this distribution as a bump that traveled downstream. Also, the dynamic stall vortex was accompanied by a reduction in the leading edge suction peak. A similar display with one of the cases utilizing the synthetic jet is shown in figure 3.23. Here the pressure-bump due to the dynamic stall vortex is seen to be larger than in figure 3.22. Figure 3.24 shows how the effect of the jet-momentum coefficient corresponded to the formation of the dynamic stall vortex. The values of the angles used in the inception of the vortex were determined from inspection of the lift and pitching moment data. These values did not occur when the vortex was formed, but rather when the lift and moment were affected. This displays that the frequency played a major role in the timing of the dynamic stall vortex.

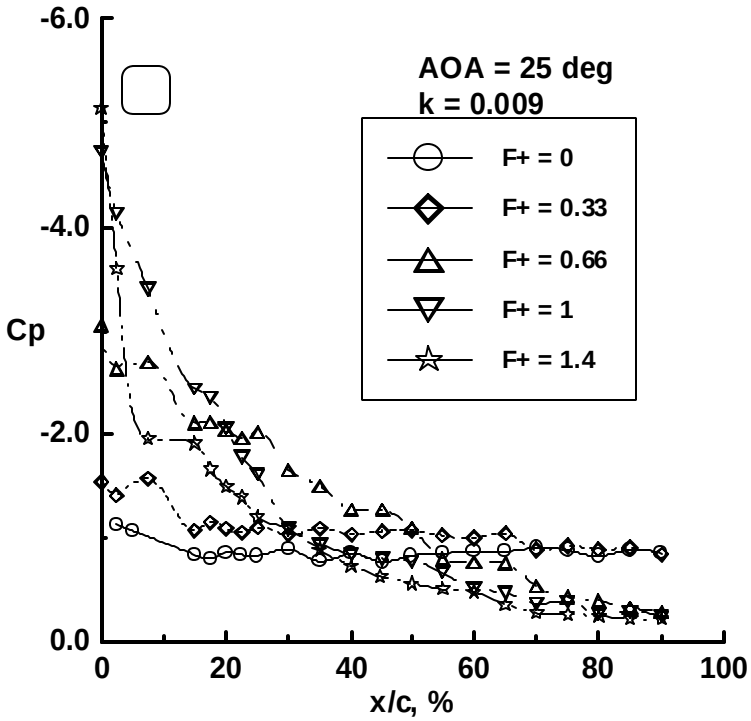

Figure 3.21. Upper Surface Pressure Distribution of Ramped Wing a=25

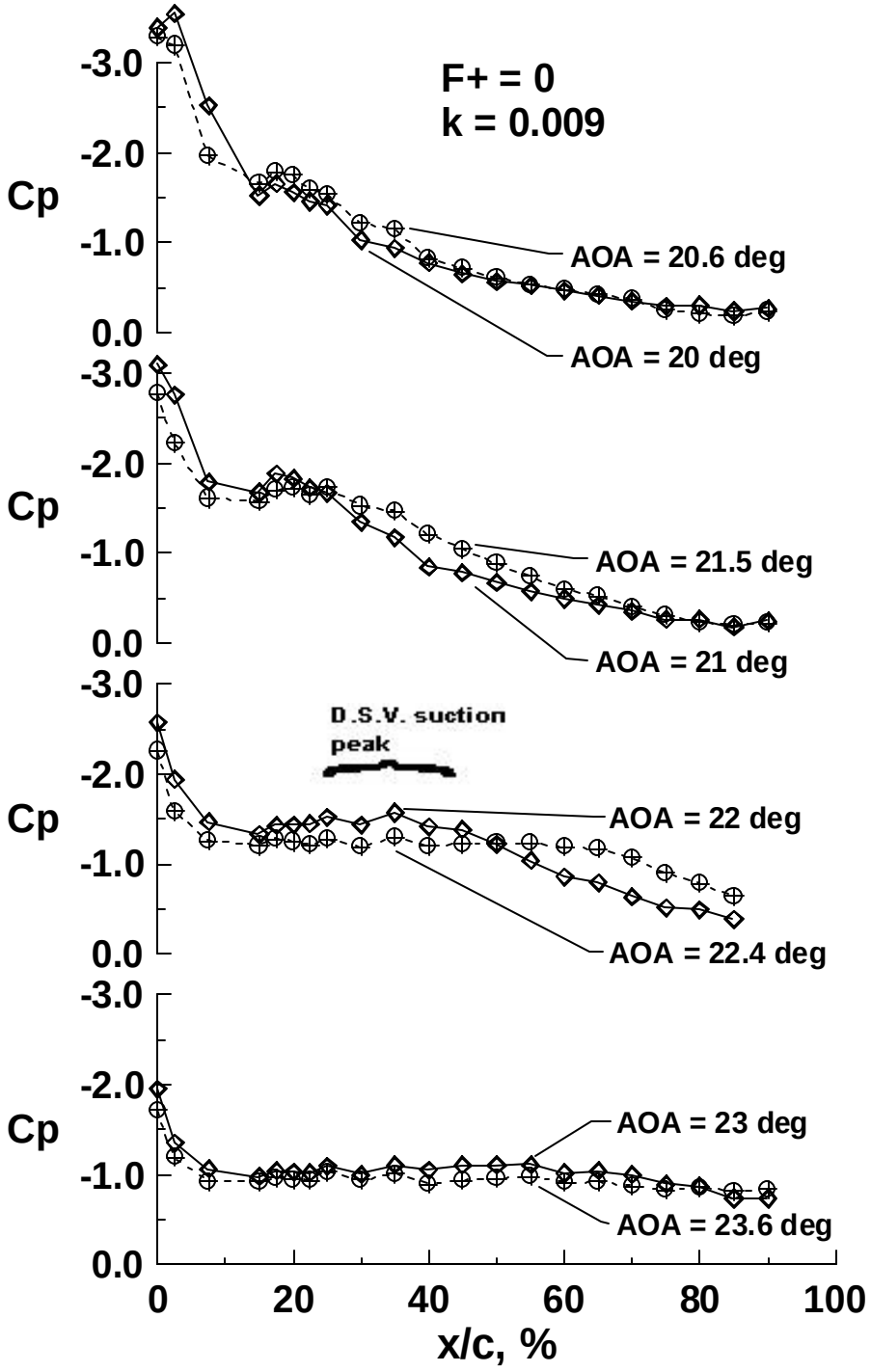

Figure 3.22 Ramping Upper Surface Pressure Distribution With No Actuation

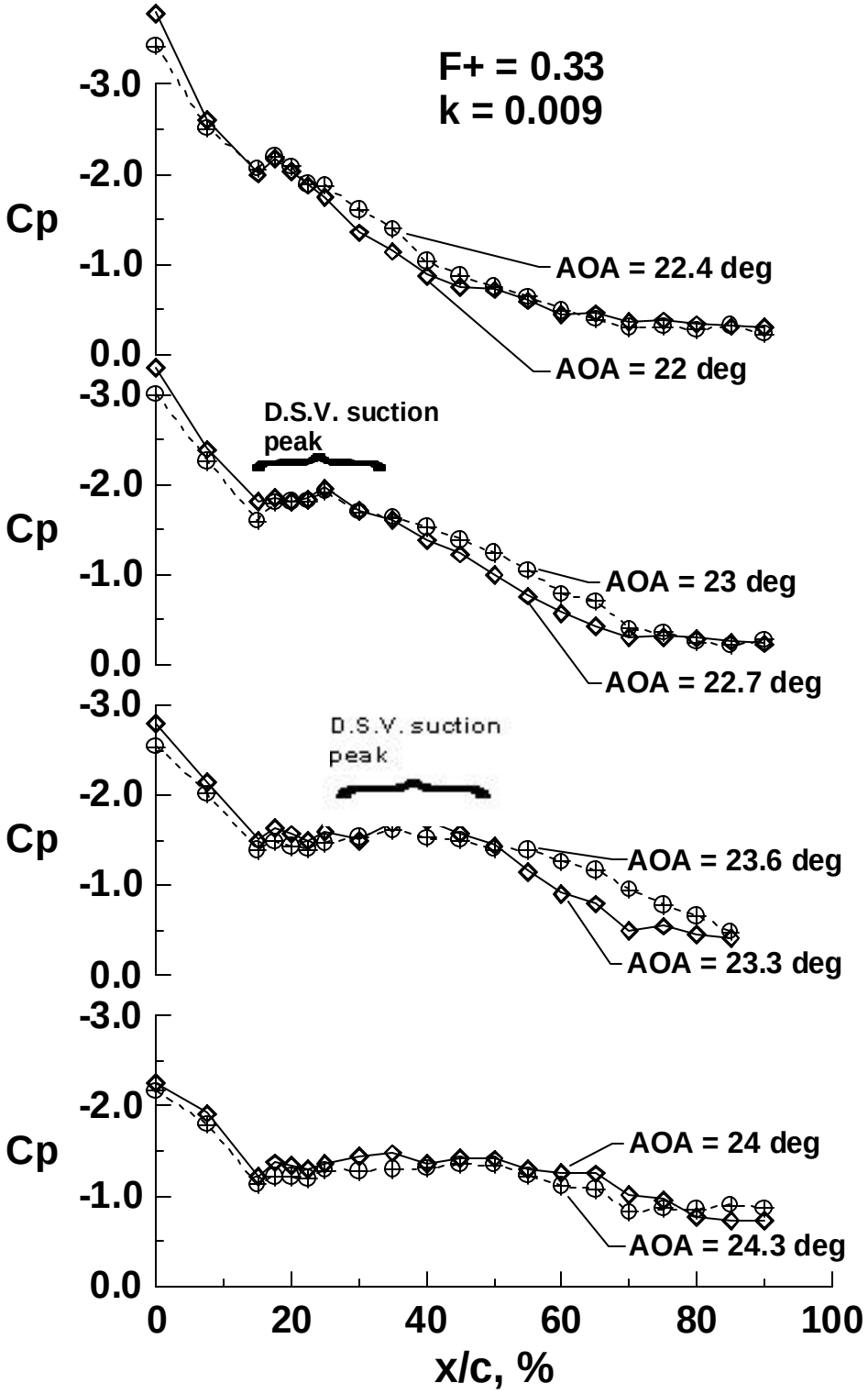

Figure 3.23 Ramping Upper Surface Pressure Distribution With Actuation

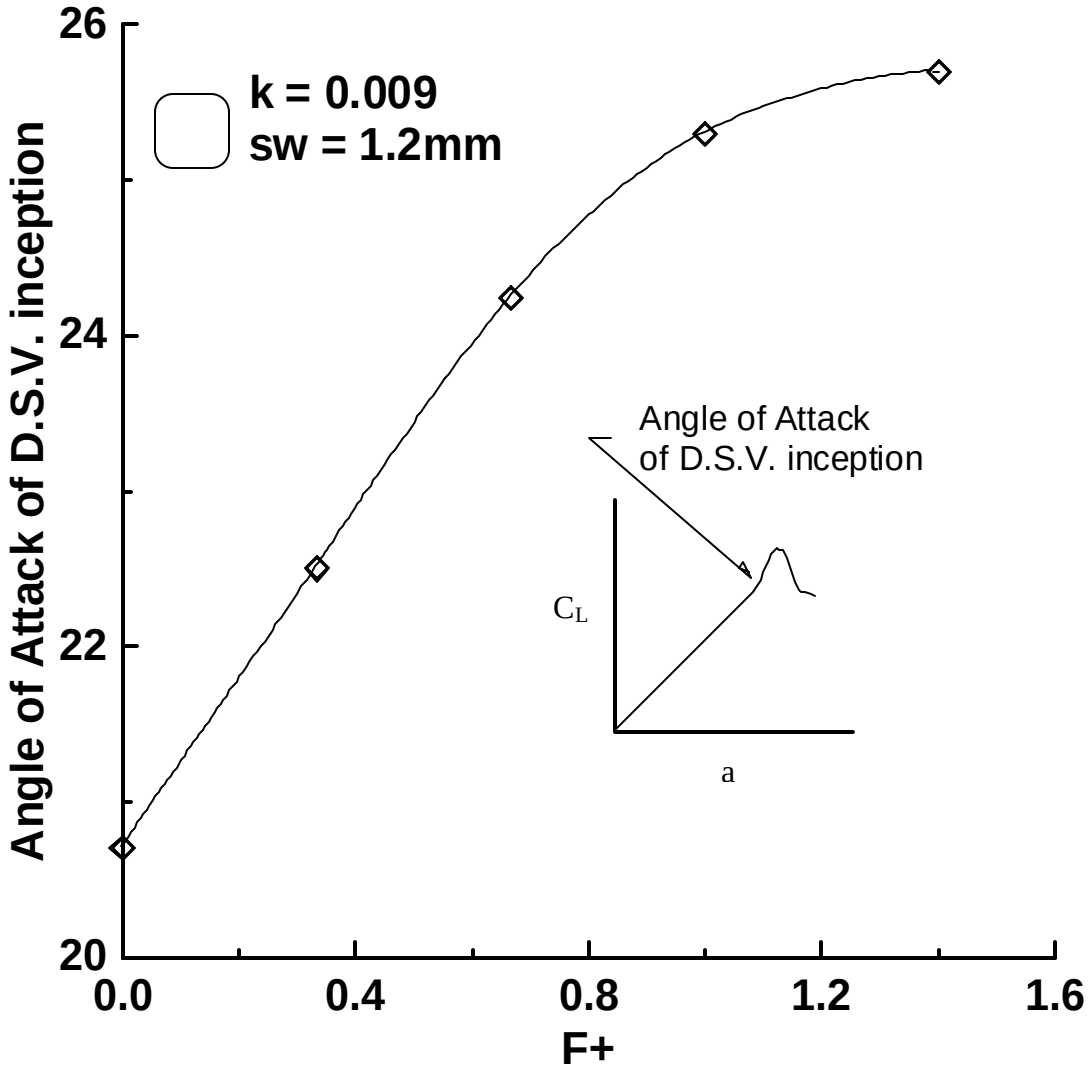

Figure 3.24 Effect of F+ on Dynamic Stall Formation

4. TRAILING EDGE SYNTHETIC JET ACTUATOR

General

This section presents the effects that a trailing edge synthetic jet actuator has upon the aerodynamic characteristics of an airfoil. The methods used to build and test the model is discussed.

Trailing Edge SJA Wing Design and Fabrication

A separate wind tunnel model was manufactured for the trailing edge test. The piston driven synthetic jet actuator was also used for the trailing edge synthetic gurney actuator. The structure of the test bed was built from machined aluminum. The NACA 0015 shape was made from pieces, built in our rapid-prototype machine, from ABS plastic and thin sheets of Plexiglas. The chord of the airfoil is 0.425 meters and the span is 0.26 meters. Also Plexiglas side plates were added to minimize the 3D effects of the airflow. The wing is displayed in figure 4.1. Trip strips were placed at a location of 5% on the upper and lower surfaces. The model was tested with and without a sharp trailing edge. Initial tests, however, showed that the exit slot could not be placed close enough to the trailing edge to obtain the desired effect when the sharp trailing edge was employed. Due to this, a configuration using the blunt trailing edge was used. Tests comparing the blunt and sharp trailing edges without the synthetic jet in the same wing have shown a negligible effect. The plenum of the trailing edge synthetic jet is illustrated in figure 4.2 and figure 4.3. The plenum "piped" the fluid from the pistons to the airfoil surface. Inside of the trailing edge there was also a flapper piece that can be rotated to switch the exit slot from the upper to the lower surface. This flapper was controlled using a model airplane actuator.

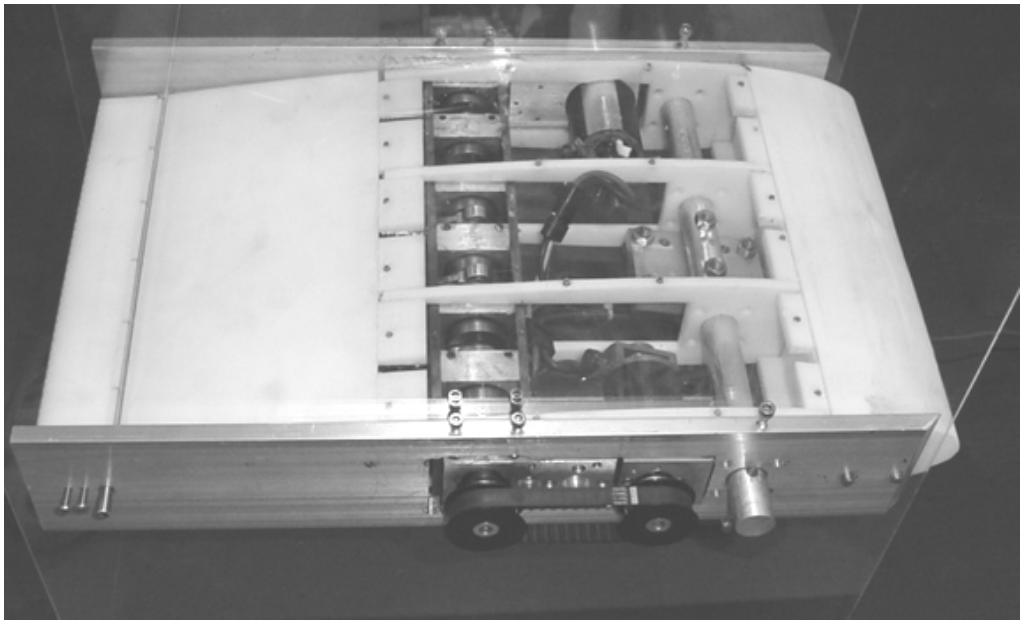

Figure 4.1 Wind Tunnel Model Showing SJA Drive Through Acrylic Access Panel

Figure 4.2 Cross Section of Trailing Edge Showing Original Plenum Design

Figure 4.3 Cross Section of Trailing Edge Showing Narrow Plenum Design

Using the TSI IFA 300 hot wire anemometer the exit velocity of the trailing edge for the different plenums and different slot widths was established. The probe was positioned approximately 0.3mm inside the slot opening for a slot width of 1.6mm and approximately 0.3mm above the slot exit for the 1mm slot exit. Table 4.1 shows the results of these tests while figures 4.4a-h show the velocity recorded as a function of time. The results of the hot wire are de-rectified to show the difference in positive and negative velocity. A positive velocity corresponded to a jet emanating from the slot. A negative velocity corresponded to a suction of fluid through the slot. The data displayed in figure 4.4 illustrates a pseudo-sinusoidal velocity time history. The inflow and the outflow appear to have fairly good symmetry. The asymmetry of the peak was probably due to compressibility effects as the velocity reaches its maximum value. The asymmetry increased as the slot width lending credence to this hypothesis.

Table 4.1 displays effects of the compressibility incurred upon the large plenum. For the large plenum an increase of the maximum velocity was not obtained with a smaller slot width. According to the conservation of mass, the velocity should have increased as the exit area was decreased. The smaller slot width actually created a slower jet at high motor speeds, an indication of extreme losses. As done previously for the leading edge case the ideal compressibility parameter value of $K = 0.00102$ was found.

Table 4.1 SJA Velocity Data Summary

Geometry	60Hz LP 1.6mm slot	100Hz LP 1.6mm slot	60Hz 1mm slot	LP	100Hz LP 1mm slot	60Hz NP 1.6mm slot	100Hz NP 1.6mm slot	60Hz 1mm NP slot	100Hz NP 1mm slot
v_{rms}, m/s	15.5	25.0	16.6		16.6	19.2	31.3	27.6	48.2
v_{max}, m/s	22	36.1	31		30.5	29.1	47.3	40.6	68.5
K	0.00059	0.00058	0.00052		0.00031	0.00078	0.00076	0.00068	0.00069
$K/K_{theoretical}$	0.58	0.57	0.51		0.31	0.76	0.75	0.67	0.68

LP=large plenum NP=narrow plenum

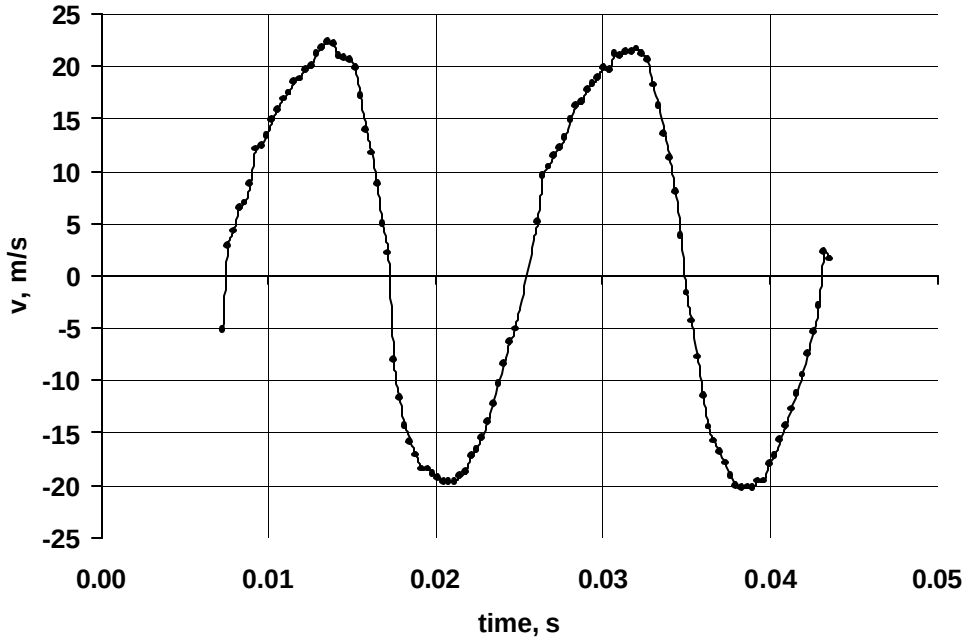

Figure 4.4a Rectified Temporal Exit Velocity Trace *sw*=1.6mm, *f*=60Hz

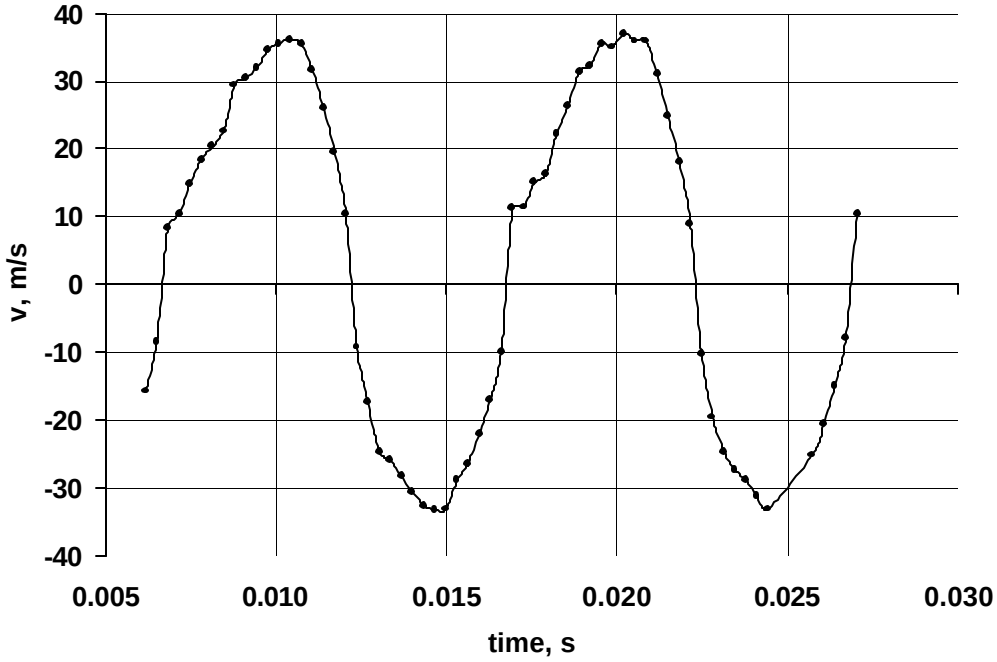

Figure 4.4b Rectified Temporal Exit Velocity Trace *sw*=1.6mm, *f*=100Hz

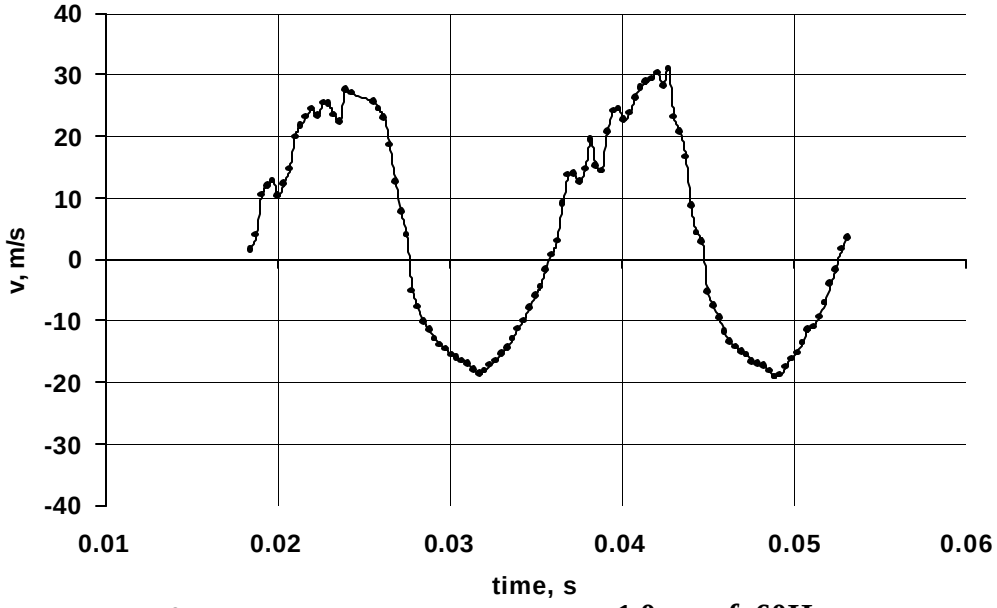

Figure 4.4c Rectified Temporal Exit Velocity Trace *sw*=1.0mm, *f*=60Hz

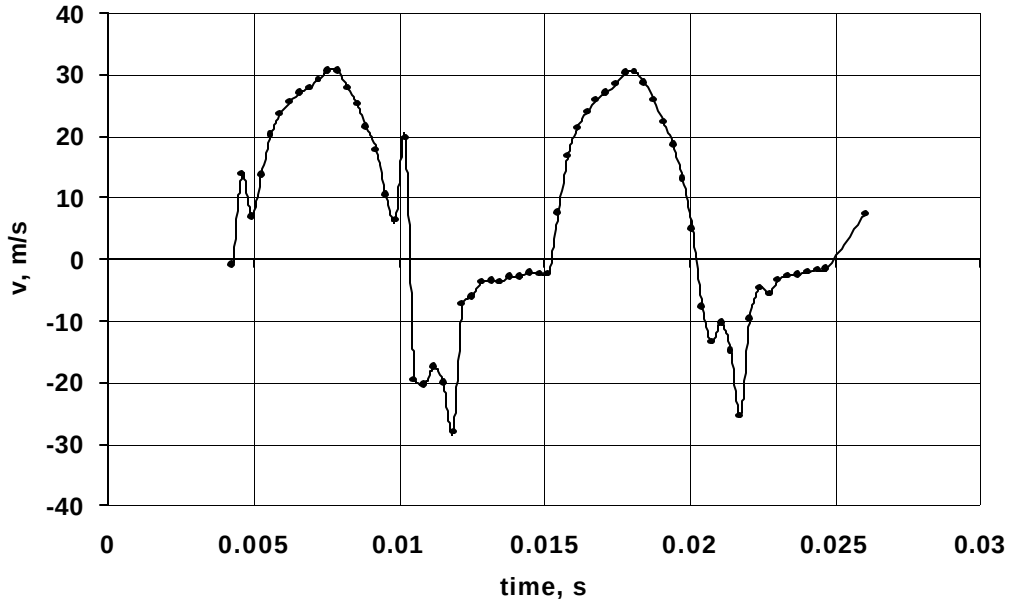

Figure 4.4d Rectified Temporal Exit Velocity Trace *sw*=1.0mm, *f*=100Hz

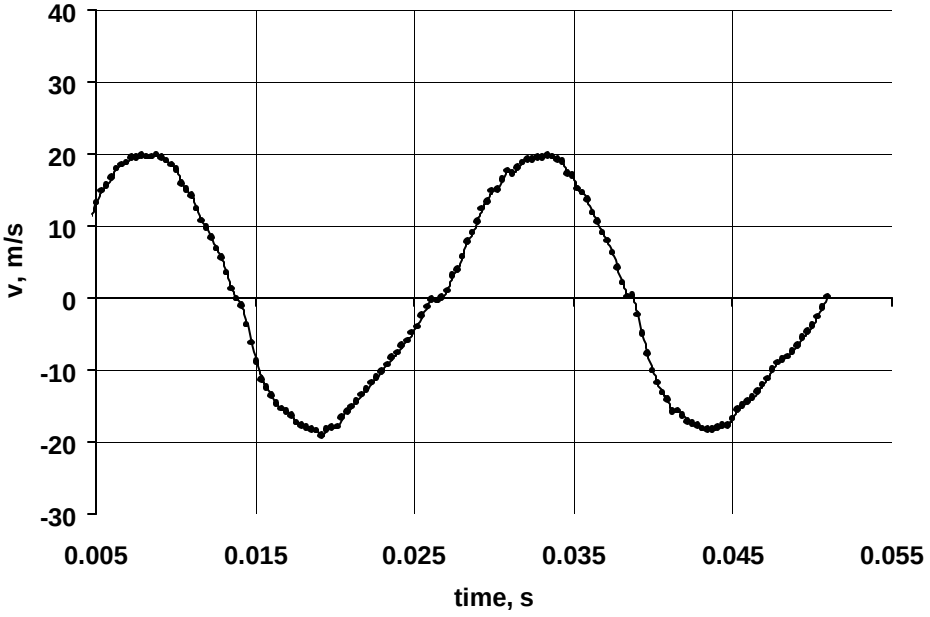

Figure 4.4e Rectified Temporal Exit Velocity Trace *sw*=1.6mm, *f*=40Hz, narrow plenum

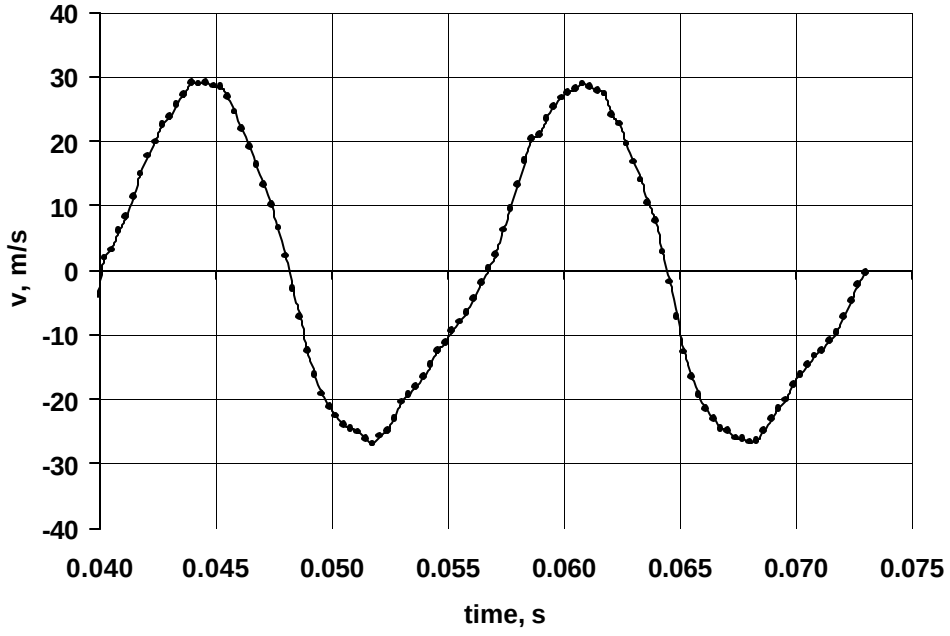

Figure 4.4f Rectified Temporal Exit Velocity Trace *sw*=1.6mm, *f*=60Hz, narrow plenum

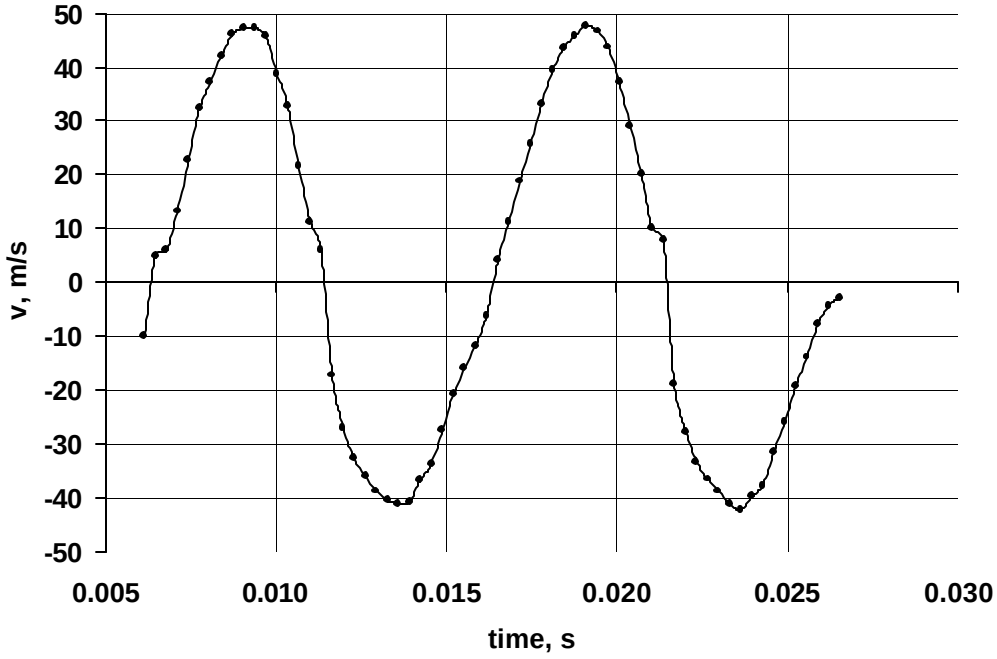

Figure 4.4g Rectified Temporal Exit Velocity Trace *sw*=1.6 mm, *f*=100Hz, narrow plenum

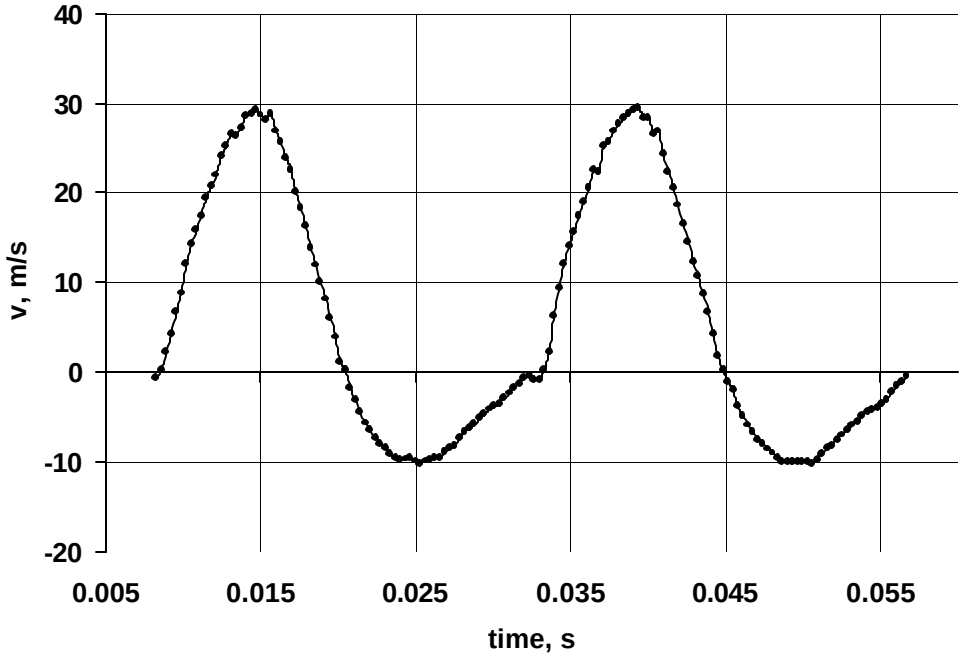

Figure 4.4h Rectified Temporal Exit Velocity Trace *sw*=1.0 mm, *f*=40Hz, narrow plenum

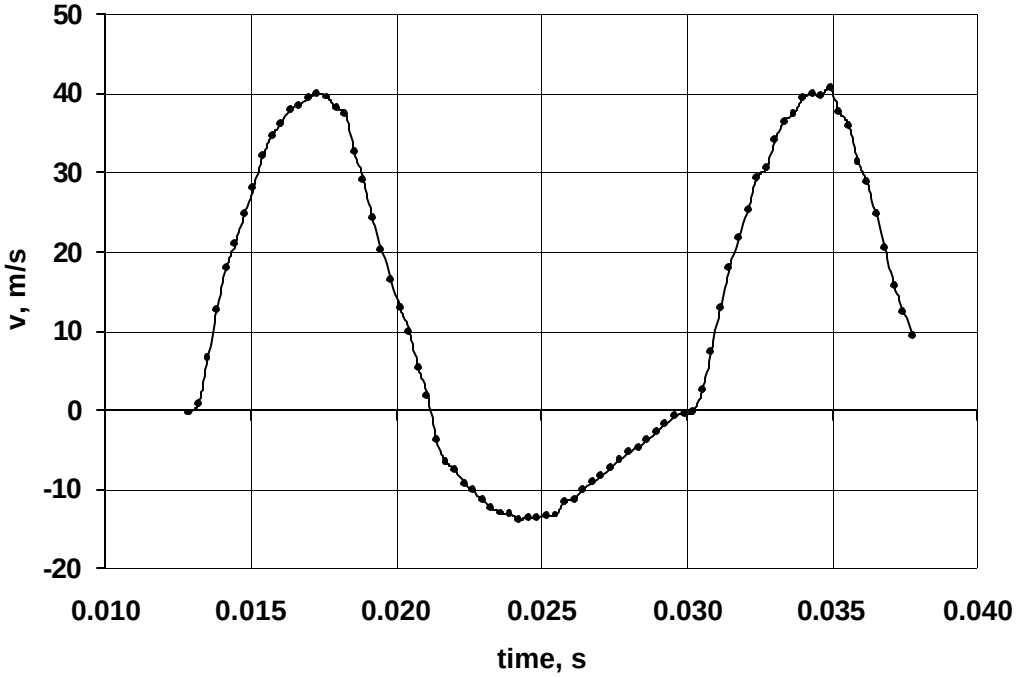

Figure 4.4i Rectified Temporal Exit Velocity Trace *sw*=1.0 mm, *f*=60Hz, narrow plenum

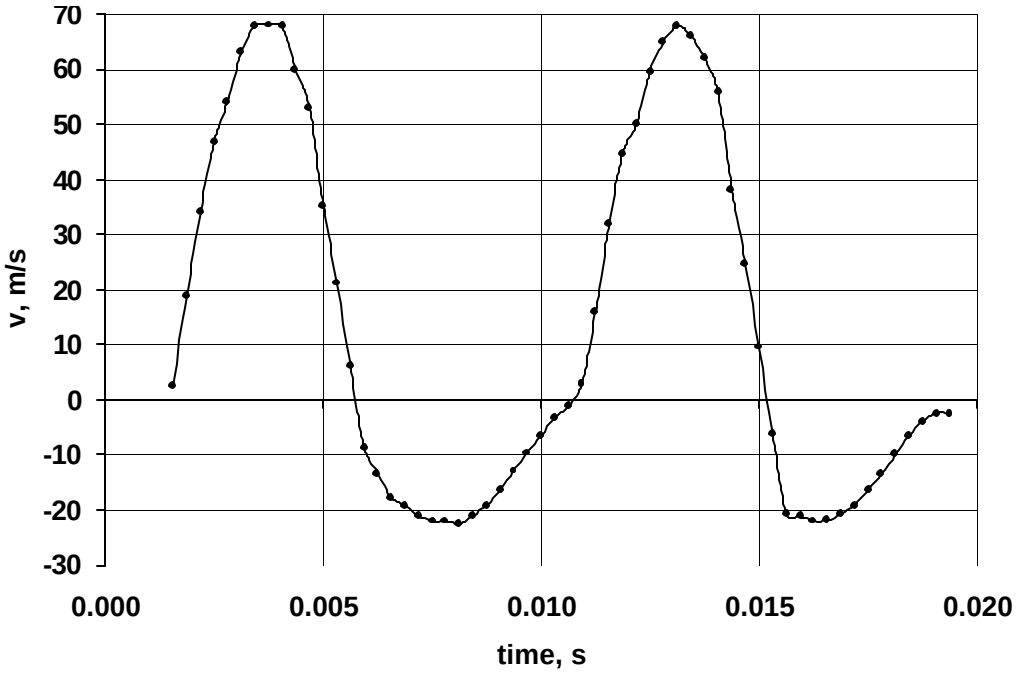

Figure 4.4j Rectified Temporal Exit Velocity Trace *sw*=1.6mm, *f*=60Hz, narrow plenum

Once again the equation for this parameter is expressed as $K = v_{\max} sw / f$. Table 4.1 includes the compressibility parameter for each of the plenums, slot widths and motor frequencies. This shows that all of the cases exhibit compressibility effects, but the effects were extreme in the case of the large plenum. For this reason most of the tests utilizing this model test bed have been performed using the smaller plenum.

Table 4.2 contains a summary of SJA operational parameters for the narrow plenum at the test velocity (20m/s). Parameters are defined as:

$C_m = 2v_{rms}^{\ 2} sw / U^2 c$ Jet momentum coefficient (4.1)

$C_{mass} = v_{rms} sw / Uc$ Mass flow coefficient (4.2)

Table 4.2 SJA Operational Parameter Summary

slot width, mm	*f*, Hz	C_μ	C_{mass}
1	40	0.0043	0.0023
1	60	0.0089	0.0033
1	100	0.027	0.0057
1.6	40	0.0033	0.0025
1.6	60	0.0069	0.0036
1.6	100	0.018	0.0059

Data repeatability was quantified in Fig. 4.5, where two data runs for the base-line wing (no SJA) are presented. In all data, the effects of the jet reaction on lift and pitching moment coefficient, Cm, have been removed through tare runs; consequently, pure aerodynamic loading is shown. Note that all the presented data is for the small (narrow) volume plenum.

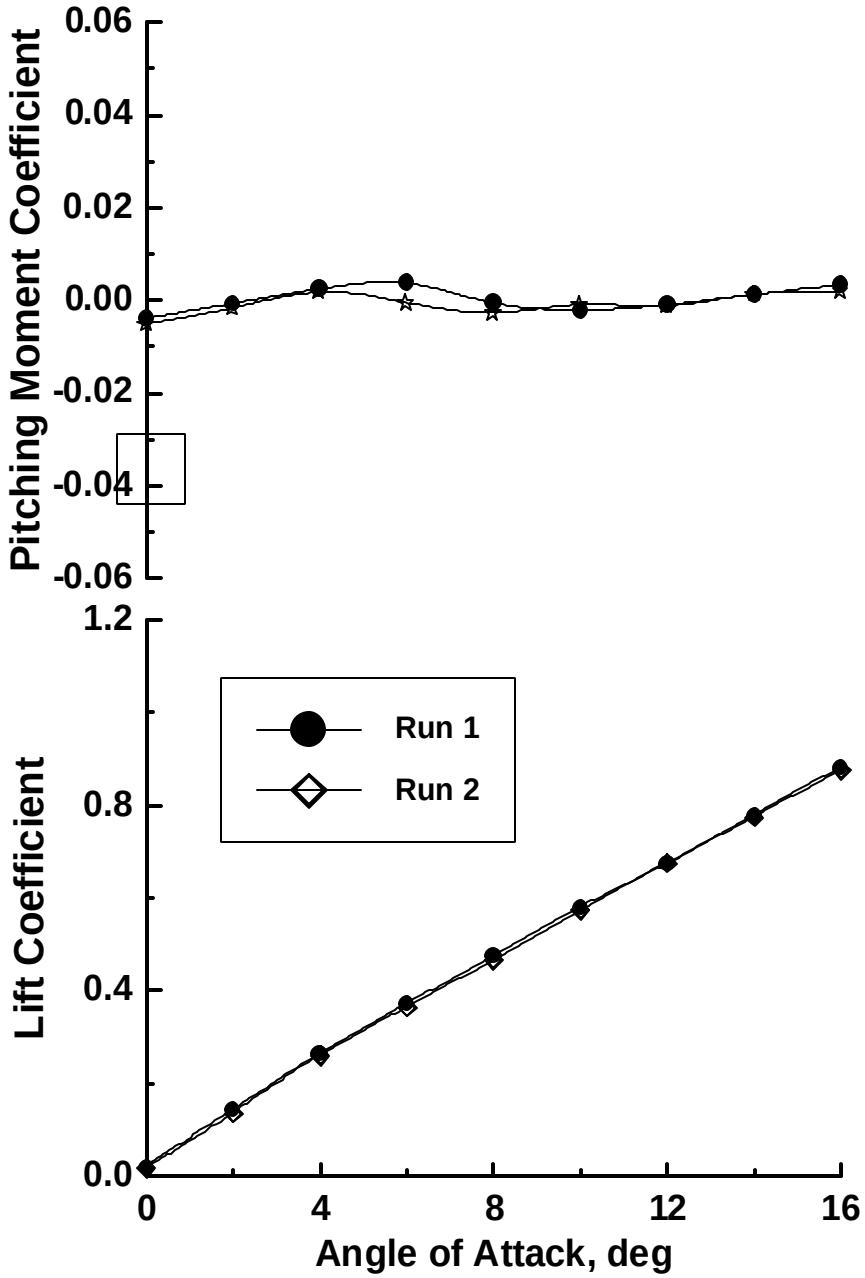

Figure 4.5 Repeated Test with No Actuation

Trailing Edge SJA Wing Results

The effect upon the aerodynamic characteristics as a function of angle of attack and jet-momentum coefficient for a 1mm slot are shown in Fig 4.6. For these tests it should be noted that the frequency of the motor was used as a parameter and not the non-dimensional frequency (F^+). With the trailing edge experimental setup the flow was assumed to be always attached. It is unlikely that any flow mechanism will be affected by the frequency ranges that were being used. The synthetic jet was also at an inefficient location to cause an effect from oscillation. Also included in Fig 4.6 is experimental data obtained from the attachment of a 1% chord Gurney flap placed at the same location as the synthetic jet slot. As seen in the figure, the trailing edge synthetic gurney flap shifted the zero angle of attack toward negative vaues. This is analogous to the result obtained for conventional flaps. Also, the result of creating a negative nose-down pitching moment corresponded to the effect of a flap on the pitching moment coefficient. For the purposes of creating "hinge-less" control over a wing it was seen that the trailing edge synthetic jet actuator creates an increase in lift and a nose down pitching moment. As seen in previous models, due to wind tunnel constraints, the side plates should have been larger and gave a smaller coefficient of lift than expected. Once again due to the comparative nature of the tests being performed this was assumed to be unimportant. To gauge the effectiveness of the synthetic jet actuator the lift augmentation ratio was examined. This ratio is defined to be $(Cl_{C\mu?0}-Cl_{C\mu=0})/C_\mu$ for the present configuration of the jet and related the effectiveness of the jet to the supplied momentum. A ratio greater than one indicated that the jet is changing the flow by an amount that is larger than by the reactive lift created from the jet. The reactive force of the jet is calculated in terms of C_μ. The figure displays that the synthetic jet has a very large value of lift augmentation when compared to the lift augmentation added from the momentum of the jet. Worth noting as well, is that the level of lift augmentation decreased as the coefficient of the jet increased. This result was expected and predicted from previous theory [36]. The effectiveness of the synthetic jet upon the lift and lift augmentation ratio were independent for the angle of attack at the pre-stall incidences.

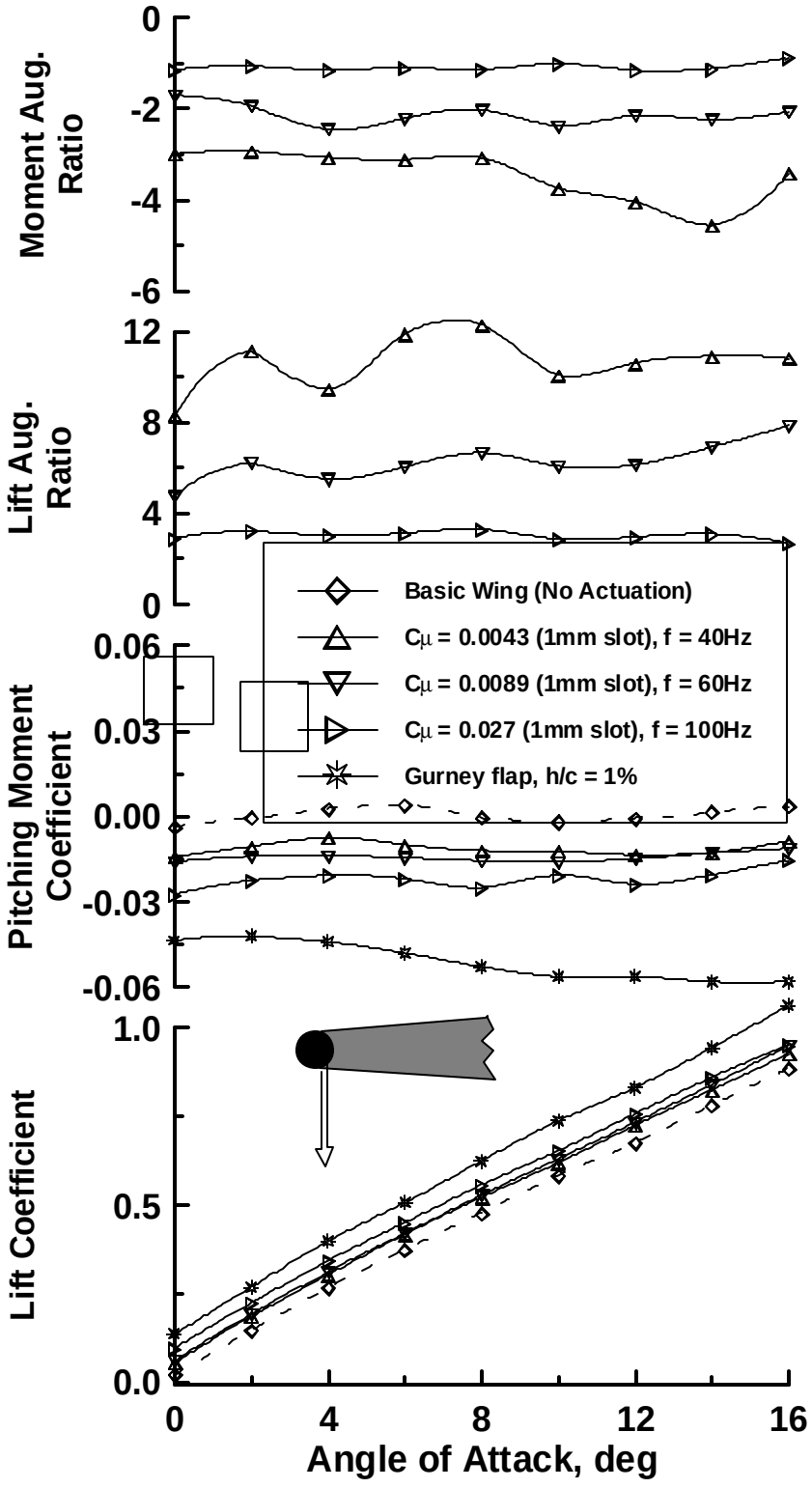

Figure 4.6 Effects of SJA Jet Flap on Measured Aerodynamic Parameters, 1mm Slot.

For “hinge-less” flow control an effective change in the moment coefficient was needed. From Figure 4.6 it can be shown that the trailing edge synthetic gurney flap produced a negative moment when compared to the case without actuation and was proportional to the C_μ of the jet. It was also noticed that at the current speeds of the synthetic jet the moment produced is smaller than that of a traditional Gurney flap. However, this produced a large enough moment to control the angle of attack of an airplane at low angles. Fig. 4.6 displays the moment augmentation ratio for the jet with a 1mm slot, also. This ratio is akin to the lift augmentation ratio and shows that for vales less than -1 the resultant moment was greater than the result from a jet alone. The moment augmentation ratio was defined to be $(Cm_{C\mu?0}-Cm_{C\mu=0})/(C_\mu(l/c))$. The distance *l* was the distance from the quarter chord to the jet exit slot. For the current model used, *l* was 0.31m, giving a value of l / *c* =0.73. The result here was the same as the result of the lift augmentation ratio in so much as that the augmentation decreased as the coefficient of blowing of the jet increased.

The data presented in figure 4.7 illustrates the same type of data as Figure 4.6 except that the slot width for this case was 1.6mm. The purpose of presenting two slot widths was to compensate for uncertainty of the setting of the slot width. The trends established for the smaller slot width can be seen in this figure. The difference in the two cases was that the effect of the jet with a larger slot width was larger even though C_μ was lower (Table 4.2). This was noticed in the lift and moment curves as well as the two augmentation curves. This leads to the suggestion that the momentum of air injected was not the only factor in the effectiveness of the synthetic jet. The shear quantity of air being sucked and blown has an effect on the system. For the lowest levels of the blowing coefficient (C_μ=0.0033) the jet created lift augmentation ratios as high as 16 and moment augmentation ratios as low as -6. The data in Figs. 4.6 and 4.7 shows that the levels of moment augmentation were generally lower then lift augmentation.

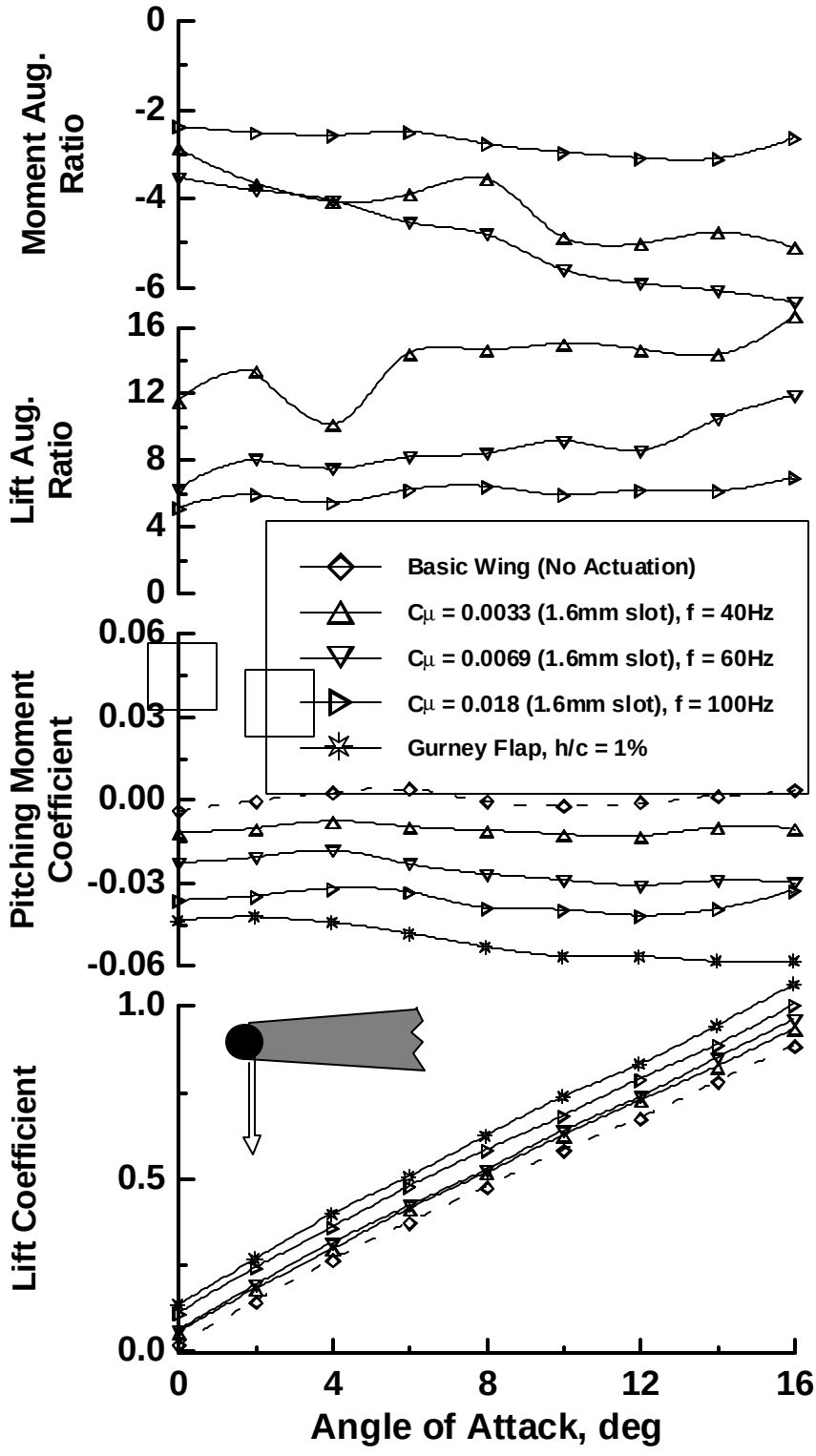

Figure 4.7 Effects of SJA Jet Flap on Measured Aerodynamic Parameters, 1.6mm Slot.

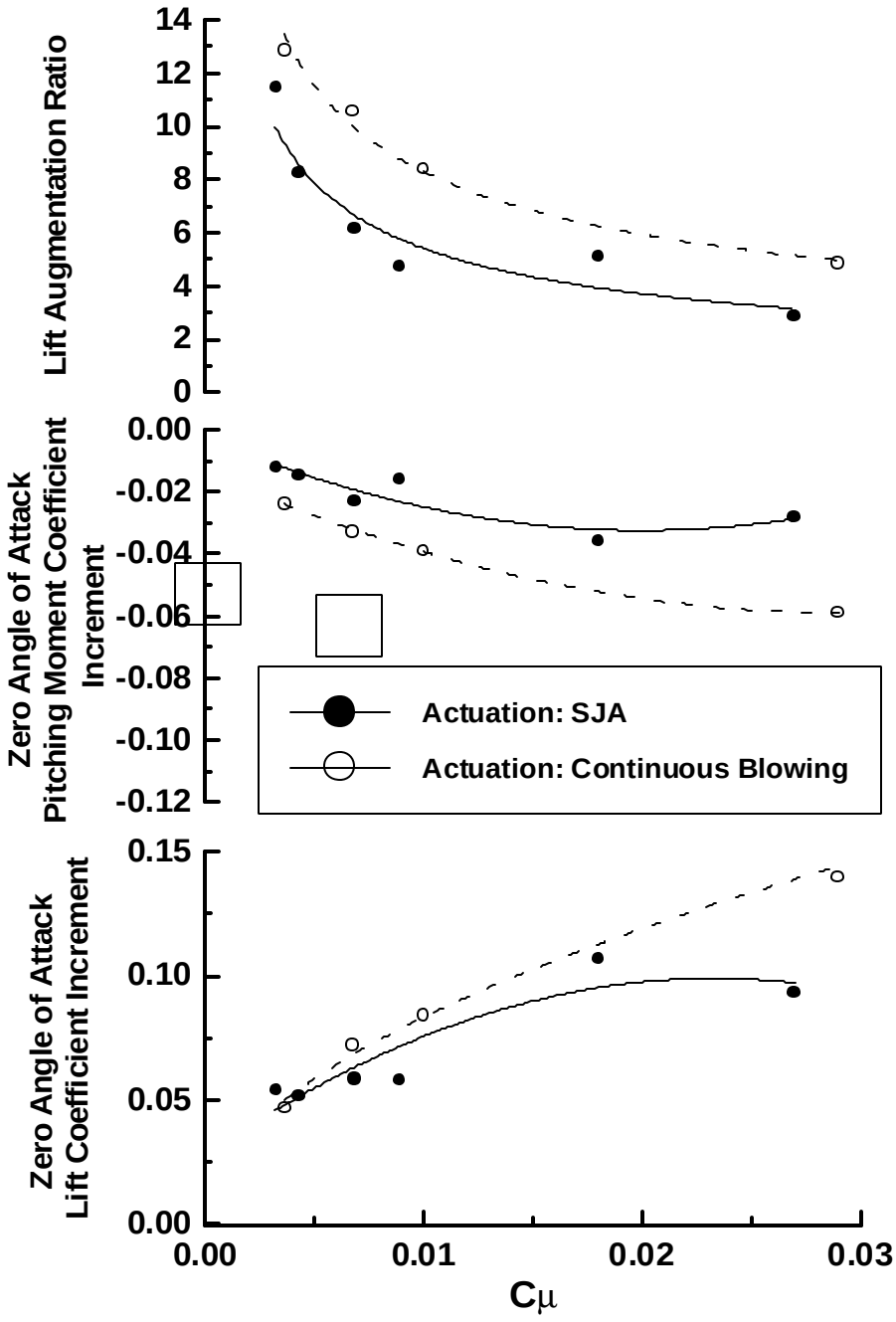

Figure 4.8 Effects of SJA Cμ on Measured Zero Angle of Attack Aerodynamic Parameters.

Figure 4.8 displays a summary of the dependence of the zero angle of attack lift, pitching moment and lift augmentation ratio on the jet momentum coefficient. The effects of continuous blowing, included in the figure, on the augmentation ratio and lifting and moment coefficients were taken from previous test by Traub et al [30]. The trends developed from this data indicated that the continuous jet was more effective than the synthetic jet for equal coefficients of blowing. Once again in the presence of attached flow the synthetic jet was unable to influence the shear layer or boundary layer receptivity mechanism. The benefits created from the use of a gurney jet are primarily the result of an increase in circulation and turning the flow around the trailing edge. This ultimately changed the rear stagnation point of the airfoil. The suction cycle of the synthetic jet gurney flap does not create any advantages in the augmentation of the circulation.

Figure 4.9 shows the data from the lift and moment coefficients from Fig. 4.8 re-plotted as a function of the mass flow rate coefficient. This data was presented without the continuous blowing data. The scatter in the data was reduced in this presentation. Although the general characteristics were similar, the form of the functional dependency (e.g. zero angle of attack lift increment as a function of the coefficient of mass) appeared different from the dependence on the mass flowrate.

To help create a larger effect on the airflow properties, the implementation of a small flap with the trailing edge synthetic jet actuator was tested. For hinge-less or "near" hinge-less flow control, the impact of the interaction of the SJA with a Gurney flap was of interest. A Gurney flap is a relatively minor structural modification. It would be useful if its performance could have been modulated using a SJA. Consequently, an experiment was undertaken where a Gurney flap was positioned either upstream (US) or downstream (DS) of the SJA exit (see the inset sketch in Fig. 4.10). The placement of the flap was such that the jet was ejected tangential to the surface of the Gurney. The data in Fig. 4.10 suggests, within the experimental accuracy, that the SJA had little effect

on the Gurney flap physics. This result was surprising as the effect of a trailing edge jet or Gurney flap on the flow physics was vastly different.

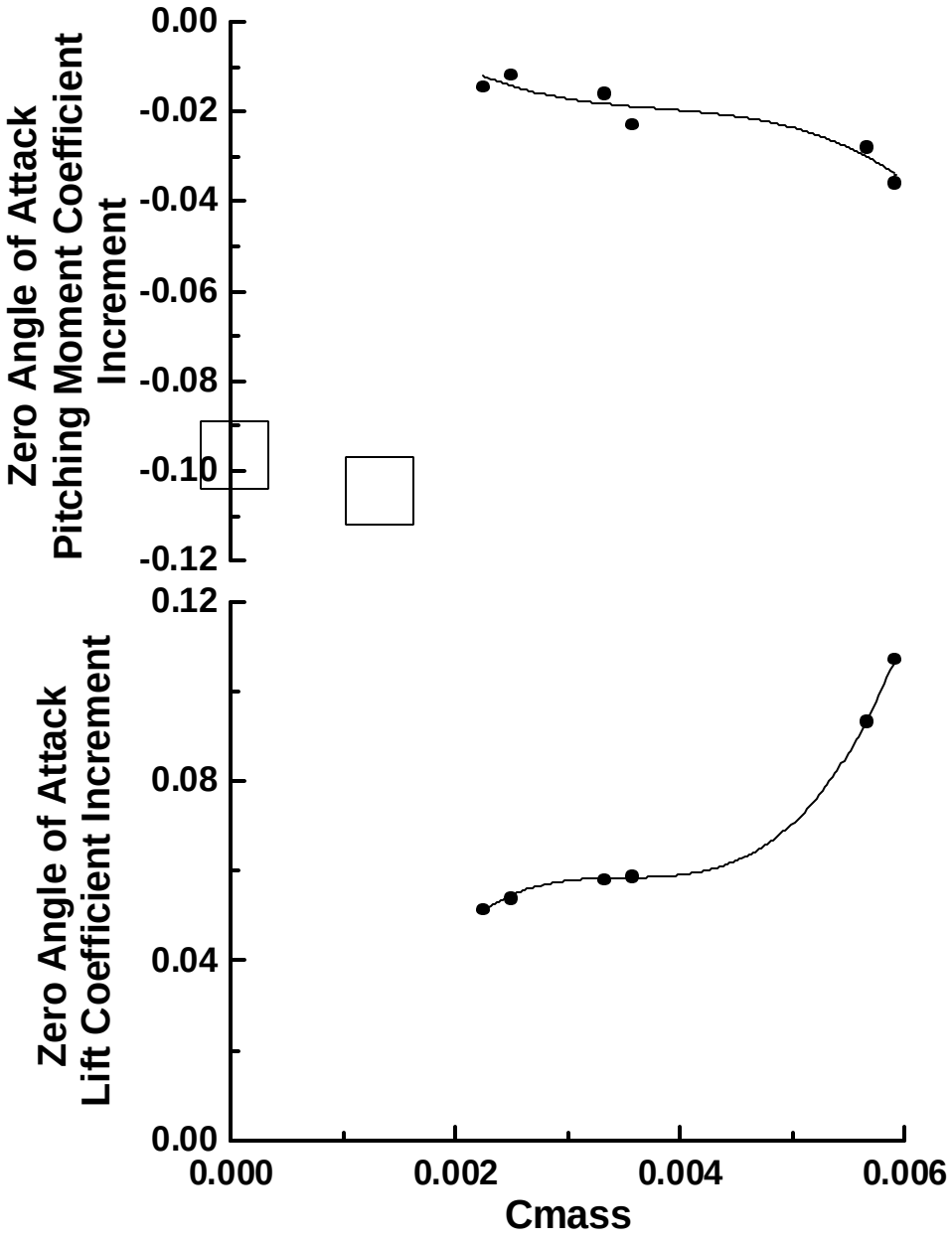

Figure 4.9 Effects of SJA Cm on Measured Zero Angle of Attack Aerodynamic Parameters.

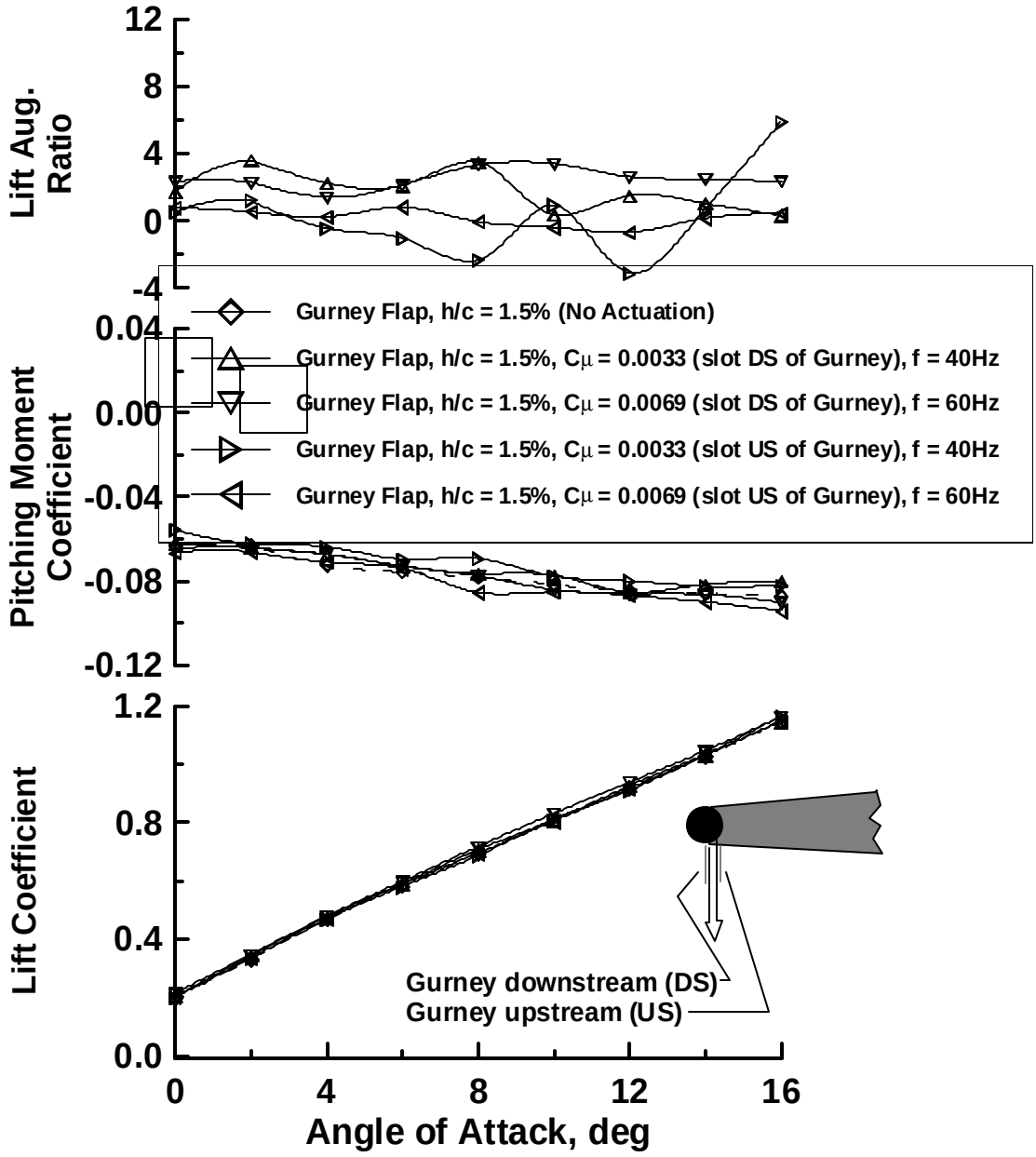

Figure 4.10 Effects of SJA Jet – Gurney Flap Combinations on Measured Aerodynamic Parameters.

5. CONCLUSIONS

This thesis presents a study of the effects of flow control on a NACA0015 airfoil using Synthetic Jet Actuators (SJA) for the purposes of flow separation delay and "hinge-less" flow control. The SJA is examined at two separate locations of the airfoil.

The synthetic jet was placed in the leading edge of a wind tunnel model wing. Experimental tests were performed for steady and pitching models. The leading edge synthetic jet effectively delayed the onset of stall from 17 degrees angle of attack to 25 degrees angle of attack. This data indicates that at high angles of attack sufficient pitching and lifting moment authority is available to posses some level of control. The use of the leading edge synthetic jet at pre-stall angles of attack provided no advantages over the performance of the wing without actuation.

A preliminary wind tunnel investigation was undertaken to examine the possibility of using a SJA-jet flap for "hinge-less" control. Preliminary tests encompassed jet momentum coefficient variation. The data indicated that with the present implementation, the SJA-jet flap generated moderate lift (0.12) and moment (0.045) coefficient increments that should be suitable for hinge-less control. It is shown that for the current experimental setup and a given jet momentum coefficient, continuous blowing was more effective then oscillatory blowing/sucking. Combining the SJA with a Gurney flap showed little performance enhancement or control.

For a wide range of angles of attack, the use of the leading and trailing edge synthetic jet could be used to possess control authority throughout the range of incidence angles. Conversely, the leading edge SJA may be used solely to delay stall, while the trailing edge SJA could be used as a driver for aerodynamic control.

REFERENCES

[1] Klausmeyer, S. M., ,Papadakis, M., and Lin, J. C., 1996, "A Flow Physics Study of Vortex Generators on a Multi-Element Airfoil," AIAA Paper 96-0548, 34th Aerospace Sciences Meeting & Exhibit, Reno, NV.

[2] Chang, R. C., Hsiao, F. B., and Shyu, R. N., 1992, "Forcing Level Effects of Internal Acoustic Excitation on the Improvement of Airfoil Performance," Journal of Aircraft, **29 (5)**, pp. 823-829.

[3] Huang, R. F., and Mao, S. W., 2002, "Separation Control on a Cantilever Wing with a Self-Excited Vibrating Rod," Journal of Aircraft, **39 (4)**, pp. 609-615.

[4] Prandtl, L., 1904, "Über Flüssigkeitsbewegugng bei sehr kleiner Reibung", Proceedings of the Third International Mathematics Congress, Heidelberg, Germany, pp.484-491.

[5] Kruger, W., 1947, "Drag Reduction By Suction of the Boundary Layer Separated Behind Shock Wave Formation At High Mach Numbers," NACA Technical Memorandum 1168.

[6] Tillman, T. G. and Hwang, D. P., 1999, "Drag Reduction on a Large-Scale Nacelle Using a Micro-Blowing Technique," AIAA 99-0130, 37th Aerospace Sciences Meeting & Exhibit, Reno, NV.

[7] Modi, V. J., Munshi, S. R., Bandyopadhyay, G., and Yokomizo, T., 1998, "High-Performance Airfoil with Moving Surface Boundary-Layer Control," Journal of Aircraft, **35 (4)**, pp. 544 –553.

[8] Sun, M., and Hamdani. H., 2001, "Separation Control by Alternating Tangential Blowing/Suction at Multiple Slots," AIAA 01-0297, 39th Aerospace Sciences Meeting, Reno, NV.

[9] Choi, K.-S., and Clayton, B. R., 2001, "The Mechanism of Turbulent Drag

Reduction With Wall Oscillation," International Journal of Heat and Fluid Flow, **22**, pp. 1-9.

[10] Ashpis, D. E., and Reshotko, E., 1990, "The Vibrating Ribbon Problem – Revisited," Journal of Fluid Mechanics, **213**, pp. 531-547.

[11] Greenblatt, D., Darabi, A., Nishri, B., and Wygnanski, I., 1998, "Separation Control By Periodic Addition of Momentum with Particular Emphasis on Dynamic Stall," Proceedings Heli Japan 98, Paper T3-4, American Helicopter Society.

[12] Greenblatt, D., and Wygnanski, I., 2001, "Dynamic Stall Control by Periodic Excitation, Part 1: NACA 0015 Parametric Study", Journal of Aircraft, **38 (3)**, pp. 430-438.

[13] Seifert, A., and Pack, L., 2000, "Dynamics of Active Separation Control at High Reynolds Numbers," AIAA Paper No. 2000-0409, 38th Aerospace Sciences Meeting & Exhibit, Reno, NV.

[14] Gilarranz, J. L. and Rediniotis, O. K., 2001, "Compact, High-Power Synthetic Jet Actuators for Flow Separation Control," AIAA Paper 2001-0737, 39th Aerospace Sciences Meeting & Exhibit, Reno, NV.

[15] Gilarranz , J. L., Traub, L. W. ,and Rediniotis, O. K., 2002, "Characterization of a Compact, High-Power Synthetic Jet Actuator for Flow Separation Control," 40th Aerospace Sciences Meeting & Exhibit, Reno, NV.

[16] Goodmanson, L. T., and Gratzer, L. B., 1973, "Recent Advances in Aerodynamics for Transport Aircraft – Part 1", Astronautics and Aeronautics, **11**, pp. 30-45.

[17] Goodmanson, L. T., and Gratzer, L. B., 1974, "Recent Advances in Aerodynamics for Transport Aircraft – Part 2", Astronautics and. Aeronautics, **12**, pp. 52-60.

[18] Gad-el-Hak, M., 2000, *Flow Control: Passive, Active, and Reactive Flow Management*, Cambridge University Press, New York, pp. 150-188.

[19] Rathnasingham, R. and Breuer, K. 1997, "Coupled Fluid-Structural Characteristics of Actuators for Flow Control," AIAA Journal, **35**, pp. 832-837.

[20] Seifert A, Eliahu S, Greenblatt D, Wygnanski I, 1998, "On the Use of Piezoelectric Actuators for Airfoil Separation Control," AIAA Journal, **36**, pp.1535-1537.

[21] Seifert, A., and Pack, L., 1999, "Oscillatory Control of Separation at High Reynolds Numbers," AIAA Journal, **37**, 1062-1071.

[22] McCormick, D., 2000, "Boundary Layer Separation Control with Directed Synthetic Jets," AIAA Paper 2000-0519, 38th Aerospace Sciences Meeting & Exhibit, Reno, NV.

[23] Traub, L.W., Miller, A., and Rediniotis, O., 2004, "Effects of Active and Passive Flow Control on Dynamic Stall Formation," Journal of Aircraft, **41 (2)**, pp. 405-408.

[24] Traub, L., Miller, A., Ukapi, U., Rediniotis, O., Jeong, G. and Kim, K., 2003, "Reconfigurable Synthetic Jet Actuation And Closed-Loop Flow Control," Paper No. AIAA 2003-0217, 41st Aerospace Sciences Meeting and Exhibit, Reno, NV.

[25] Liebeck, R. H., 1978, "Design of Subsonic Airfoils for High Lift," Journal of Aircraft, **15 (9)**, pp. 547-561.

[26] Jang, C. S., Ross, J. C., and Cummings, R. M., 1992, "Computational Evaluation of an Airfoil with a Gurney Flap," AIAA Paper 92-2708, 30th Aerospace Sciences Meeting & Exhibit, Reno, NV.

[27] Papadakis, M., Myose, R. Y., Heron, I., and Johnson, B. L., 1996, "An Experimental Investigation of Gurney Flaps on a GA(W)-2 Airfoil with 25% Slotted Flap," AIAA Paper 96-2437, 34th Aerospace Sciences Meeting & Exhibit, Reno, NV.

[28] Jeffrey, D. Zhang, X., and Hurst, D. W., 2000, "Aerodynamics of Gurney Flaps on a Single-Element High-Lift Wing," Journal of Aircraft, **37 (2)**, pp. 295-301.

[29] Bloy, A. W., Tsioumanis, N., and Mellor, N. T., 1997, "Enhanced Aerofoil Performance using Trailing-Edge Flaps," Journal of Aircraft, **34 (4)**, pp. 569-571.

[30] Traub, L.W., Miller, A., and Rediniotis, O., 2004, "Comparisons of a Gurney and Jet Flap for Hingeless Control," Journal of Aircraft, **41 (2)**, pp. 420-422.

[31] Rae, W., and Pope, A., 1984, *Low-speed Wind tunnel Testing*, John Wiley and Sons, New York, pp. 344-401.

[32] Johansen, E. S., Dec. 2001, "Development of a Fast-Response Multi-hole Probe for Unsteady and Turbulent Flowfields," Ph.D. dissertation, Aerospace Engineering Department, Texas A&M University, College Station.

[33] Wildhack, W.A., 1937, "Pressure Drop in Tubing in Aircraft Instrument Installations," NACA TN-593, pp. 30.

[34] Amitay, M., and Glezer, A., 2002, "Role of Actuation Frequency in Controlled Flow Reattachment over a Stalled Airfoil," AIAA Journal, **40 (2)**, pp. 209-216.

[35] Lorber, P., McCormick, D., Anderson, T., Wake, and MacMartin, B., 2000, "Rotorcraft Retreating Blade Stall Control," AIAA Paper 2000-2475, 38th Aerospace Sciences Meeting & Exhibit, Reno, NV.

[36] Spence, D. A., 1958, "Some Simple Results for Two-Dimensional Jet-Flap Aerofoils," The Aeronautical Quarterly, November, pp. 395-406.

VITA

Adam Cole Miller

PO Box 7335, College Station, TX 77844

(979) 2206122 – (979) 8458170

e-mail: acm5638@neo.tamu.edu

EDUCATION:

2000- 2004 Master of Science Degree in Aerospace Engineering at Texas A&M University (College Station, Texas). GPR: 3.55 / 5.00.

1995- 2000 Bachelor of Science Degree in Aerospace Engineering at Texas A&M University (College Station, Texas). GPR: 3.43 / 5.00.

PROFESSIONAL EXPERIENCE:

2001- Present Department of Aerospace Engineering, Texas A & M University.
Graduate Research Assistant. Flow Control via Synthetic Jet Actuators.

2000- 2001 PIC Components (Brenham, Texas).
Design Engineer. Design of pressure seals.

PUBLICATIONS:

Traub, L. W., Miller, A. C., and Rediniotis, O.K., "Effects of Synthetic Jet Actuation on a Pitching NACA 0015 Wing, Journal of Aircraft**,**, Vol. 41, No. 5, 2004, pp. 1153-1162.

Traub, L. W., Miller, A. C., and Rediniotis, O.K., "Effects of Active and Passive Flow Control on Dynamic Stall Vortex Formation," Journal of Aircraft, Vol. 41, No. 2, 2004, pp. 405-408

Traub, L. W., Miller, A. C., and Rediniotis, O.K., "Comparison of a Gurney and Jet-Flap for Hinge-Less Control," Journal of Aircraft, Vol. 41, no. 2, 2004, pp. 420-423.

Traub, L. W., Miller, A. C., and Rediniotis, O.K., "Effects of Synthetic Jets on Large Amplitude Sinusoidal Pitch Motions," Journal of Aircraft**,** accepted for publication.

Traub, L.W, Miller, A.C., and Rediniotis, O., "Investigation of a Synthetic Jet Flap for Pitch Control," in preparation.

Traub, L.W, Miller, A.C., and Rediniotis, O., "Gurney Flap Dependencies; an Experimental Investigation," in preparation.